

1 **Response to comments:**

2 We sincerely thank the reviewer for the helpful comments. In the text that follows, reviewer
3 comments in normal text are followed by author responses in italics.

4

5 **Comment 1:**

6 I urge the authors to reconsider the discussion regarding wet removal (Referee 1 specific
7 comment 6; lines 977-986, 999-1006 in the revised track changes version). In particular, the
8 authors need to more convincingly show that there is a connection between wet removal (rain,
9 fog, etc.) and high LWC (the addition of precipitation to figure 1 does not adequately show this).
10 Regarding the variation in MO-OOA with LWC (Figure 7), given the large variability in
11 MO-OOA in each bin, it does not appear to me that there are any robust trends. I urge the authors
12 to consider how robust the trends are and add discussion regarding this to lines 999-1006. Also,
13 could the results be explained by changes in production rather than changes in removal?

14

15 *Response:*

16 *We thank the reviewer for bring this point to our attention again. The total cloud cover (%) from*
17 *Air Resources Laboratory's data archive on the website of NOAA's READY Archived*
18 *Meteorology (<https://ready.arl.noaa.gov/READYamet.php>) for the measurement location were*
19 *added to Figure 1 (A, F). The relative humidity was likely high when the total cloud cover was*
20 *significantly high, which could decrease the production of OOA or enhance its removal. Text has*
21 *been modified appropriately.*

22

23 *We have added the correlation coefficient of MO-OOA vs. LWC to denote the robustness of the*
24 *variation trend in MO-OOA with LWC.*

25

26 *Our revisions are included in the following bulleted list:*

27 *1. The previous discussion (original lines 999-1006) has been revised as follows (lines 450-456*
28 *in the revised manuscript):*

29 *“MO-OOA slightly increased during both seasons as LWC increased (Fig. 7 (I, J)). In winter,*
30 *MO-OOA presents an increasing trend from 0.57 to 0.98 $\mu\text{g m}^{-3}$ when LWC increased from 2.5 to*
31 *40 $\mu\text{g m}^{-3}$ but decreased as the LWC increased further. The slope of this increase was*
32 *approximately 0.008 $\mu\text{g MO-OOA } \mu\text{g}^{-1}$ LWC with correlation coefficient of 0.55. In summer,*
33 *MO-OOA appears to increase from 0.49 to 0.64 $\mu\text{g m}^{-3}$ when LWC increased from 2.5 to 27.5 μg*

34 m^{-3} , with slope of $0.005 \mu\text{g MO-OOA } \mu\text{g}^{-1} \text{ LWC}$ ($R^2=0.34$). In winter, because of the decrease in
35 LO-OOA with LWC, the relative fraction of MO-OOA increases as LWC increases.”

36

37 2. We added another statement regarding the comparison of the varying trend of MO-OOA with
38 LWC during nighttime and whole periods (lines 484-485):

39 “The nighttime increasing trends of MO-OOA against LWC in both seasons are stronger than
40 those shown in Fig. 7(I, J) in terms of the correlation coefficient values.”

41

42 3. We altered phrasing regarding changes in production versus removal in several locations.

43

44 **Comment 2:**

45 In regards to Referee 1 specific comment 7, I also find the discussion regarding MSA confusing.
46 It would help if the authors incorporated some of their response to the referee into the revised
47 version of the manuscript.

48

49 *Response:*

50 *Our discussion regarding MSA suggested that the summertime MO-OOA formation was more*
51 *likely associated with aqueous processing than LO-OOA as MO-OOA positively correlated with*
52 *MSA but LO-OOA exhibited weak correlation with MSA. However, as suggested by Referee 1*
53 *specific comment 7, it is entirely possible for aqueous processing to produce OOA and at the*
54 *same time for the OOA factors to exhibit weak (or no) correlations with MSA (e.g., if the air*
55 *mass had a continental origin). Thus, we deleted the discussion relevant to MSA in the updated*
56 *manuscript.*

57

58 **Comment 3:**

59 Lines 894-896: What exactly is meant by “more prominent”? More mass or a larger fraction of
60 total sulfate production? Have the authors considered other explanations that could account for
61 this?

62

63 *Response:*

64 *We have rephrased the sentence as follows on lines 347-350:*

65 *“By comparing the diurnal plots of sulfate in winter and summer, it appears that sulfate*
66 *generated from aqueous chemistry accounted for more mass and a greater fraction of total*

67 *sulfate production in winter than in summer.”*

68

69 **Comment 4:**

70 Line 964: “likely results” It should be possible to directly calculate this and make a more
71 definitive statement.

72

73 *Response on lines 412-416:*

74 *The correlation coefficients have been calculated and added in the statement that provide a more*
75 *explicit explanation about the statement:*

76 *“It should be noted that a fit for the binned data likely results in an increase in R^2 compared to*
77 *the fit for the original data. For example, the correlation coefficient of the fit for the averaged*
78 *binned wintertime MO-OOA (increased from 0.57 to 0.98 $\mu\text{g m}^{-3}$) versus LWC (increased from*
79 *2.5 to 40 $\mu\text{g m}^{-3}$) is 0.55, while it is 0.06 for the original data (Figure 7(I)).”*

80

81 **Comment 5:**

82 Several sections of the manuscript need to be revised to clarify that the results are a correlation
83 and not definitive proof that a specific process is happening. Specific examples include (line
84 numbers refer to track changes version):

85 Lines 977-986 (see above comment regarding production vs loss)

86

87 *Response:*

88 *Changes have been made throughout the document to achieve these clarifications and soften the*
89 *language used.*

90

91 **Comment 6:**

92 Lines 1011-1012: What about the role of NO_3 chemistry? How is that separated from
93 aqueous-phase chemistry at night? Was the role of carryover (influence of daytime production)
94 explored?

95

96 *Response:*

97 *We presumed that the NO_3 chemistry is probably linked with aqueous-phase chemistry. A*
98 *previous study reported that the partitioning of organic compounds to the particle phase was*
99 *significantly increased at elevated RH levels (70%) in an urban area dominated by biogenic*

100 *emissions in Atlanta (Hennigan et al., 2008). From our data, the correlation of ON and LO-OOA*
101 *in summer nighttime ($r=0.76$) was stronger than that during daytime (0.53). The concurrent*
102 *enhancement of the LWC and nitrate functionality from organic nitrate during nighttime*
103 *demonstrates that the LWC does not inhibit increases in ON concentration, as might be expected*
104 *if hydrolysis of ON occurred rapidly. This is included in the text on lines 502-505.*

105 *The importance of carryover of daytime production of water-soluble organic gases (WSOG) and*
106 *their effect on aq-SOA depends on the expected atmospheric lifetime or uptake reversibility of*
107 *WSOG (Hodas et al. 2014). This is also true of semi-volatile organic products that partition as a*
108 *function of temperature. Given that the measurement of either gas-phase water-soluble or*
109 *semi-volatile organic compounds was not included in this work, it is not possible to comment on*
110 *this possibility in this dataset.*

111

112 **Comment 7:**

113 Lines 1048-1050: The statement that aerosol water facilitates formation of ON needs to be
114 supported. In general, hydrolysis is thought to be a sink of ON. Couldn't this be due to higher
115 organic nitrate yields from $\text{NO}_3 + \text{BVOC}$ chemistry compared to $\text{OH} + \text{BVOC}$ chemistry?

116 *Response:*

117 *We thank the referee for highlighting this fact. The original statement has been rephrased as*
118 *follows, now on lines 500-505:*

119 *“This is likely due to the higher ON yields from NO_3^- -initiated chemistry involving BVOCs*
120 *during nighttime compared to hydroxyl radical + BVOCs chemistry during daytime. Additionally,*
121 *the concurrent enhancement of the LWC and nitrate functionality from organic nitrate during*
122 *nighttime demonstrates that the LWC likely does not inhibit increases in ON concentration.”*

123

124 **Comment 8:**

125 Resolution of the figures needs to be improved (particularly the time series figures). They are
126 currently difficult to read.

127 *Response:*

128 *The figures have been updated with high resolution.*

129

130 **References**

131 *Hennigan, C. J., Bergin, M. H., Dibb, J. E., and Weber, R. J.: Enhanced secondary organic*
132 *aerosol formation due to water uptake by fine particles, Geophys. Res. Lett., 35, L18801,*

133 <http://doi.org/10.1029/2008gl035046>, 2008.
134 Hodas, N., Sullivan, A. P., Skog, K., Keutsch, F. N., Collett Jr, J. L., Decesari, S., Facchini, M. C.,
135 Carlton, A. G., Laaksonen, A., and Turpin, B. J.: *Aerosol Liquid Water Driven by*
136 *Anthropogenic Nitrate: Implications for Lifetimes of Water-Soluble Organic Gases and*
137 *Potential for Secondary Organic Aerosol Formation*, *Environ. Sci. Technol.*, 48, 19,
138 11127-11136, 2014.

139 **Seasonal differences in formation processes of oxidized organic aerosol near**

140 **Houston, TX**

141 Qili Dai^{1, 2}, Benjamin C. Schulze^{2, 3}, Xiaohui Bi^{1, 2}, Alexander A.T. Bui², Fangzhou Guo², Henry

142 W. Wallace^{2, 4}, Nancy P. Sanchez², James H. Flynn⁵, Barry L. Lefer^{5, 6}, Yinchang Feng^{1*}, Robert J.

143 Griffin^{2, 7}

144 ¹ State Environmental Protection Key Laboratory of Urban Ambient Air Particulate Matter Pollution

145 Prevention and Control, College of Environmental Science and Engineering, Nankai University, Tianjin

146 300350, China

147 ² Department of Civil and Environmental Engineering, Rice University, Houston, TX, 77005

148 ³ Now at Department of Environmental Science and Engineering, California Institute of Technology,

149 Pasadena, CA, 91125

150 ⁴ Now at Washington State Department of Ecology, Lacey WA, 98503

151 ⁵ Department of Earth and Atmospheric Sciences, University of Houston, Houston, TX, 77004

152 ⁶ Now at Division of Tropospheric Composition, NASA, Washington, DC, 20024

153 ⁷ Department of Chemical and Biomolecular Engineering, Rice University, Houston, TX, 77005

154

155 *Corresponding author: Yinchang Feng (fengyc@nankai.edu.cn)

156

157 **Abstract**

158 Submicron aerosol was measured to the southwest of Houston, Texas during winter and
159 summer 2014 to investigate its seasonal variability. Data from a high-resolution time-of-flight
160 aerosol mass spectrometer (HR-ToF-AMS) indicated that organic aerosol (OA) was the largest
161 component of non-refractory submicron particulate matter (NR-PM₁) (on average, $38 \pm 13\%$ and
162 $47 \pm 18\%$ of the NR-PM₁ mass loading in winter and summer, respectively). Positive matrix
163 factorization (PMF) analysis of the OA mass spectra demonstrated that two classes of
164 oxygenated OA (less and more-oxidized OOA, LO and MO) together dominated OA mass in
165 summer (77%) and accounted for 39% of OA mass in winter. The fraction of LO-OOA (out of
166 total OOA) is higher in summer (70%) than in winter (44%). Secondary aerosols
167 (sulfate+nitrate+ammonium+OOA) accounted for ~76% and 88% of NR-PM₁ mass in winter
168 and summer, respectively, indicating NR-PM₁ mass was driven mostly by secondary aerosol
169 formation regardless of the season. The mass loadings and diurnal patterns of these secondary
170 aerosols show a clear winter/summer contrast. Organic nitrate (ON) concentrations were
171 estimated using the NO_x⁺ ratio method, with contributions of 31-66% and 9-17% to OA during
172 winter and summer, respectively. The estimated ON in summer strongly correlated with LO-OOA
173 ($r=0.73$) and was enhanced at nighttime.

174 The relative importance of aqueous-phase chemistry and photochemistry in processing OOA
175 was investigated by examining the relationship of aerosol liquid water content (LWC) and the
176 sum of ozone (O₃) and nitrogen dioxide (NO₂) (O_x=O₃+NO₂) with LO-OOA and MO-OOA. The
177 processing mechanism of LO-OOA apparently ~~depended on~~ was related to relative humidity
178 (RH). In periods of RH <80%, aqueous-phase chemistry likely played an important role in the

179 formation of wintertime LO-OOA, whereas photochemistry promoted the formation of
180 summertime LO-OOA. For periods of high RH >80%, these effects were opposite those of low
181 RH periods. Both photochemistry and aqueous-phase processing appear to facilitate increases in
182 MO-OOA formation-concentration except during periods of high LWC, which is likely a result
183 of wet removal during periods of light rain or a negative impact on its formation rate.

184 The nighttime increases of MO-OOA during winter and summer were 0.013 and 0.01 μg
185 MO-OOA per μg of LWC, respectively. The increase of LO-OOA was larger than that for
186 MO-OOA, with increase rates of 0.033 and 0.055 μg LO-OOA per μg of LWC at night during
187 winter and summer, respectively. On average, the mass concentration of LO-OOA in summer
188 was elevated by nearly 1.2 $\mu\text{g m}^{-3}$ for a ~ 20 μg change in LWC, which was accompanied by a 40
189 ppb change in O_x .

190

191 **1 Introduction**

192 Tropospheric particulate matter (PM) has adverse effects on air quality, visibility, and
193 ecosystems and participates in climate forcing (Watson, 2002; Grantz et al., 2003; Racherla and
194 Adams, 2006; Tai et al., 2010; Liu et al., 2017). The various effects of PM depend on its physical,
195 chemical and optical properties, which are determined by its emission, formation and
196 evolution/aging processes. Atmospheric PM can either be directly emitted from primary sources
197 (fossil fuel combustion, soil dust, sea salt, biomass burning, etc.) or formed through chemical
198 reactions of gaseous precursors, as is the case for secondary inorganic sulfate (SO_4^{2-}) and nitrate

199 (NO₃⁻) and secondary organic aerosol (SOA). Understanding the source contributions and
200 formation pathways of PM is essential for mitigating its effects (Jimenez et al., 2009).

201 Houston, TX, is of great interest to the scientific community with respect to air quality, as it
202 is the fourth most populous city in the United States (U.S.) and is well known for its energy and
203 chemical industries. Numerous efforts, from modelling (McKeen et al., 2009; Li et al., 2015;
204 Ying et al., 2015) to field measurements (for example, TexAQS 2000 and II (Bates et al., 2008;
205 Parrish et al., 2009; Atkinson et al., 2010), Go-MACCS (McKeen et al., 2009; Parrish et al.,
206 2009), TRAMP2006 (Mao et al., 2010; Cleveland et al., 2012), GC-ARCH (Allen and Fraser,
207 2006), SHARP (Olague et al., 2014), and DISCOVER-AQ (Bean et al., 2016; Leong et al.,
208 2017)) have been made in the Houston metropolitan area during the past two decades, providing
209 critical insights into our understanding of air quality and atmospheric chemistry with respect to
210 the sources and formation of PM. Previous field campaigns underscore that OA accounts for a
211 major fraction of non-refractory submicron PM (NR-PM₁) in Houston (Bates et al., 2008;
212 Russell et al., 2009; Cleveland et al., 2012; Brown et al., 2013; Bean et al., 2016; Leong et al.,
213 2017; Wallace et al., 2018). The spatial variation of NR-PM₁ in Houston was investigated by
214 Leong et al. (2017), who divided greater Houston into two zones based on marked differences in
215 NR-PM₁ levels, characteristics, and dynamics measured at 16 sampling locations. Zone 1 is
216 northwest of Houston and is dominated by SOA likely driven by nighttime biogenic organic
217 nitrate (ON) formation. Intensive attention has been paid recently to such
218 anthropogenic-biogenic interactions (Bahreini et al., 2009; Bean et al., 2016). Zone 2 is the
219 industrial/urban area south/east of Houston. Wallace et al. (2018) found mobile source exhaust

220 and petrochemical emissions likely are the most important factors impacting the NR-PM₁ and
221 trace gases at a site in Zone 2.

222 Formation of SOA in clouds and the aqueous phase of aerosol particles has been reported
223 worldwide (Lim et al., 2010; Ervens et al., 2011; Xu et al., 2017). Given that both photochemical
224 oxidation and aqueous-phase chemistry are conducive to the formation of SOA, it is of interest to
225 compare the relative importance of photochemistry and aqueous-phase chemistry for SOA
226 formation in different seasons. The roles of photochemistry and aqueous-phase processing on
227 SOA formation and evolution in different seasons in Beijing have been investigated by Hu et al.
228 (2016) and Xu et al. (2017). Generally, aqueous-phase processing has a dominant influence on
229 the formation of more oxidized SOA and photochemistry plays a major role in the formation of
230 less oxidized SOA in summer and winter in Beijing, while the relative importance of these two
231 pathways in the formation processes of SOA in autumn is different from those in summer and
232 winter. The relative roles of aqueous-phase and photochemical processes in the formation of
233 SOA likely vary with location and time. The seasonal differences in the spectral patterns,
234 oxidation degrees and contributions of SOA may result from different volatile organic compound
235 (VOC) precursors, meteorological conditions and atmospheric oxidizing capacity, which are not
236 well understood in Houston, particularly in different seasons.

237 This study presents observations of NR-PM₁ from two high-resolution time-of-flight **AMS**
238 **aerosol mass spectrometer** (HR-ToF-AMS) measurement campaigns conducted during the winter
239 and summer of 2014 at a site in the suburbs of Houston, where industrial and vehicular emission
240 sources and photochemical processes are likely to play an important role in NR-PM₁ formation
241 (Leong et al., 2017). In addition to local emissions, this site was possibly impacted by regional

242 marine aerosol transported from the Gulf of Mexico (Schulze et al., 2018). The aims of this work
243 are to (1) investigate the seasonal characteristics of NR-PM₁ in the Houston area, (2) characterize
244 the primary and secondary sources by applying positive matrix factorization (PMF) analysis to
245 the measured OA mass spectra, and (3) evaluate the seasonal dependence of SOA composition
246 and formation, with a main focus on the relative effects of photochemistry and aqueous-phase
247 chemistry.

248

249 **2 Materials and Methods**

250 **2.1 Sampling Site and Campaigns**

251 Instrumentation was deployed in the University of Houston/Rice University Mobile Air
252 Quality Laboratory (MAQL), as described in Leong et al. (2017) and Wallace et al. (2018). The
253 winter campaign was conducted from February 3 through February 17, 2014, and the summer
254 campaign was conducted from May 1 to May 31, 2014. The measurement site was located on the
255 campus of University of Houston Sugar Land (UHSL) (29.5740 °N, 95.6518 °W). The campus is
256 situated southwest of downtown and the Houston Ship Channel (HSC). The map of the
257 measurement site is presented in Fig. S1 in the Supplemental Information (SI). The nearby
258 interstate highway (I-69) extends to the west of downtown and serves as a major traffic emission
259 source. The W.A. Parish Generating Station, a coal-fired power plant that is the largest
260 electricity generating facility in Texas, is ~6 miles south of the site (Fig. S1). The data collected
261 in the winter campaign are limited in duration; thus, the following discussion focuses primarily

262 on the summer campaign. The label of “winter/summer” in the text denotes the measurement
263 period in the winter/summer.

264 **2.2 Measurements**

265 The data used in this paper are reported in local time, which is 6 and 5 hours behind
266 Universal Coordinated Time in winter and summer, respectively. The details regarding the
267 instrumental setup and data processing of these measurements were the same as described in
268 Wallace et al. (2018). The NR-PM₁ composition was measured using an Aerodyne
269 HR-ToF-AMS (DeCarlo et al., 2006; Canagaratna et al., 2007). A PM_{2.5} Teflon®-coated cyclone
270 inlet was installed above the MAQL at a height of 6 m above ground to remove coarse particles
271 and to introduce air into the sampling line at a rate of 16.7 SLPM. A Nafion dryer (Perma Pure,
272 LLC) was mounted upstream of the HR-ToF-AMS to dry the sample to below 45% relative
273 humidity (RH). Particles are focused into a narrow beam via an aerodynamic lens and
274 accelerated under high vacuum into the particle sizing measurement chamber. After passing the
275 particle sizing chamber, the non-refractory components are flash vaporized at near 600°C and
276 ionized using electron impact at 70 eV. Ionized mass fragments are then transmitted directly into
277 the time-of-flight region so that the mass spectra can be obtained. In this study, the
278 HR-ToF-AMS was operated in “V-mode” to obtain the non-refractory chemical components
279 with a higher sensitivity, lower mass spectral resolution compared to the “W-mode.” Ionization
280 efficiency (IE) calibration was performed monodisperse ammonium nitrate (NH₄NO₃) at the
281 beginning and end of each campaign. Filtered ambient air was sampled every two days for
282 approximately 20 to 30 min to provide a baseline of signal for the HR-ToF-AMS during

283 campaigns. The detection limits, (Table S1 in the SI) were calculated by multiplying the standard
284 deviations of the filter periods by three.

285 Trace gas mixing ratios and meteorological parameters also were measured on the MAQL
286 during the campaigns. Carbon monoxide (CO) was measured with high-resolution cavity
287 enhanced direct-absorption spectroscopy (Los Gatos Research, Inc.), and sulfur dioxide (SO₂)
288 was quantified using a pulsed fluorescence analyzer (ThermoFischer Scientific, model 43i-TLE).
289 Nitric oxide (NO) and nitrogen dioxide (NO₂) were measured with a chemiluminescence monitor
290 with an ~~UV-LED~~ultraviolet-light-emitting-diode NO₂ photolytic converter on the NO₂ channel
291 (AQD, Inc.) The total reactive nitrogen (NO_y) was measured with a Thermo 49c-TL with a
292 heated ~~Mo~~molybdenum inlet converter. Ozone (O₃) mixing ratio was measured with ultraviolet
293 absorption (2BTech, Inc., model 205). Meteorological parameters including ambient temperature,
294 solar radiation, RH, wind speed (WS), and wind direction (WD) were measured using an RM
295 Young meteorological station. Precipitation totals from a nearby Texas Commission on
296 Environmental Quality (TCEQ) monitor site (EPA Site: 48_157_0696) were downloaded from
297 the TCEQ website. The total cloud cover data were downloaded from the READY Archived
298 Meteorology website of the National Oceanic and Atmospheric Administration.

299

300 **2.3 Data Processing**

301 The HR-ToF-AMS data analysis was performed using SQUIRREL v.1.56A and PIKA
302 v.1.19D in Igor Pro 6.37 (Wave Metrics Inc.). The relative IEs were applied to OA (1.4), SO₄²⁻
303 (1.2), NO₃⁻ (1.1), NH₄⁺ (4.0), and chloride (Cl⁻, 1.3) following the standard data analysis

304 procedures. The composition-dependent collection efficiency was applied to the data based on
305 Middlebrook et al. (2012). Elemental ratios (H/C, O/C and N/C, where H is hydrogen, C is
306 carbon, and N is nitrogen) and the ratio of organic mass to organic carbon (OM/OC) were
307 generated using the procedures described by Canagaratna et al. (2015). Example data are shown
308 in Figure S2.

309 **2.3.1 Quantification of the contributions of ON ~~and Methanesulfonic Acid (MSA)~~**

310 ~~*Estimation of ON.*~~ The mass loading of NO_3^- measured by HR-ToF-AMS includes both
311 organic and inorganic NO_3^- . The fragmentation ratio of NO_2^+ to NO^+ (NO_x^+ ratio) is different for
312 ON and inorganic NO_3^- (Farmer et al., 2010; Fry et al., 2013), and the NO_2^+ and NO^+ mass
313 loadings for ON ($\text{NO}_{2,ON}$ and NO_{ON}) can be estimated using the method proposed by Farmer et al.
314 (2010):

$$315 \quad \text{NO}_{2,ON} = \frac{\text{NO}_{2,obs} \times (R_{obs} - R_{\text{NO}_3\text{NH}_4})}{R_{ON} - R_{\text{NO}_3\text{NH}_4}} \quad (1)$$

$$316 \quad \text{NO}_{ON} = \text{NO}_{2,ON} / R_{ON} \quad (2)$$

317 where R_{obs} is the ambient NO_x^+ ratio (0.531 and, 0.260 for the winter and summer campaign,
318 respectively; see Fig. S3 for details). $R_{\text{NO}_3\text{NH}_4}$ (NO_x^+ ratio of NH_4NO_3) is determined by IE
319 calibration using monodisperse NH_4NO_3 before and after the campaigns. The average of the two
320 IE calibrations was used as the $R_{\text{NO}_3\text{NH}_4}$ for the campaign (0.588 and, 0.381 for the winter and
321 summer campaigns, respectively), which is comparable with the value reported elsewhere (Xu et
322 al., 2015; Zhu et al., 2016). The value of R_{ON} is hard to determine because it varies with
323 instruments and precursor VOCs (Fry et al., 2013). Previous studies found that isoprene was the
324 main biogenic VOC (BVOC) in Houston (Leuchner and Rappengluck, 2010; Kota et al., 2014),

325 and Brown et al. (2013) reported that monoterpenes and isoprene were frequently present within
 326 the nocturnal boundary layer in the Houston area and underwent rapid oxidation, mainly by nitrate
 327 radical (denoted as NO_3^\cdot with a dot to differentiate it from aerosol NO_3^-). Given the abundance of
 328 monoterpene and isoprene in the Houston area, similar to Xu et al. (2015), we assume organic
 329 nitrates formed via isoprene and beta-pinene oxidation are representative. Fry et al. (2013)
 330 assumed that the $R_{ON}/R_{\text{NH}_4\text{NO}_3}$ value is instrument-independent, and further estimated the
 331 average $R_{ON}/R_{\text{NH}_4\text{NO}_3}$ of 2.25 for the organic nitrate standards. The $R_{ON}/R_{\text{NH}_4\text{NO}_3}$ values vary
 332 with precursor VOC. We utilized the $R_{ON}/R_{\text{NH}_4\text{NO}_3}$ of isoprene (2.08, (Bruns et al., 2010)) and
 333 beta-pinene organic nitrates (3.99, (Boyd et al., 2015)) from the literature to obtain an estimation
 334 range of R_{ON} by using the NO_x^+ method.

335 The measured NO_x^+ ratio can be used to separately quantify ammonium and organic nitrates
 336 as:

$$337 \quad ON_{frac} = \frac{(R_{obs} - R_{\text{NO}_3\text{NH}_4})(1 + R_{ON})}{(R_{ON} - R_{\text{NO}_3\text{NH}_4})(1 + R_{obs})} \quad (3)$$

338 The nitrate functionality from organic nitrate was calculated as:

$$339 \quad \text{NO}_{3,ON} = ON_{frac} \times \text{NO}_3^- \quad (4)$$

340 Thus, the nitrate functionality from inorganic nitrate (assuming NH_4NO_3 is the solely important
 341 inorganic nitrate in the submicron mode) can be calculated as:

$$342 \quad \text{NO}_{3,AN} = (1 - ON_{frac}) \times \text{NO}_3^- \quad (5)$$

343 The accurate estimation of the total mass of ON via this method is uncertain as the actual
 344 molecular weight of the particle-phase species is unclear. The mass range of ON is estimated by
 345 assuming that the average molecular weights of organic molecules with nitrate functional groups
 346 are 200 to 300 g mol^{-1} (Surratt et al., 2008; Rollins et al., 2012). Previous work found that the

347 NO₃[·] reaction with monoterpenes resulted in significant SOA formation and that a hydroperoxy
348 nitrate (C₁₀H₁₇NO₅) was likely a major NO₃[·]-oxidized terpene product in the southeastern U.S.
349 (Ayres et al., 2015). Here, we use the molecular weight of C₁₀H₁₇NO₅ (231 g mol⁻¹) to calculate
350 the ON mass. Example periods of significant ON contribution to PM are given in Fig. S4. While
351 the values of ON concentration estimated using this method are presented in the text, the result
352 of estimated ON including uncertainties is available in Table S2.

353 ~~Estimation of methane sulfonic acid (MSA). During the two campaigns, there is no~~
354 ~~significant organic sulfur contribution from ion fragments other than CH₃SO₂⁺. The~~
355 ~~concentration of MSA was estimated as:-~~

$$356 \quad C_{MSA} = \frac{C_{CH_3SO_2^+}}{f_{MSA,CH_3SO_2^+}} \quad (6)$$

357 ~~where $C_{CH_3SO_2^+}$ is the concentration of ion fragment CH₃SO₂⁺ ($m/z=78.99$) and the fraction of~~
358 ~~CH₃SO₂⁺ to the total signal intensity of all the fragments of pure MSA, $f_{MSA,CH_3SO_2^+}$, is 5.55%.~~
359 ~~This values was observed for the mass spectra of pure MSA in laboratory experiments (Schulze~~
360 ~~et al., 2018) and is comparable to previous work (Huang et al., 2015).~~

361 2.3.2 PMF Analysis

362 The PMF technique has been used widely for source apportionment (Paatero and Tapper,
363 1994), including with HR-TOF-AMS data (Ulbrich et al., 2009; Zhang et al., 2011). The
364 high-resolution NR-PM₁ OA mass spectra matrix (mass-to-charge ratio, $m/z = 12$ to $m/z = 130$)
365 and the associated error matrix obtained by using PIKA v 1.19 D were used for PMF analysis.
366 Data were prepared according to the protocol proposed by Ulbrich et al. (2009) and Zhang et al.

367 (2011) prior to PMF analysis. The PMF model was used to decompose the measured OA mass
368 spectra matrix by solving:

$$369 \quad X = GF + E = \sum_{p=1}^J G_{ip}F_{pj} + E_{ij} \quad (76)$$

370 where X is the $m \times n$ matrix of measurement data, the m rows of X are the OA mass spectra
371 measured at each time step, the n columns of X are the time series of each organic m/z , and p is
372 the number of factors. G_{ip} is the matrix that denotes the contributions of factor p at time step i ,
373 and F_{pj} represents the factor mass spectral profiles. E is the residual matrix. The least-squares
374 algorithm is used to fit the data to minimize iteratively a quality of fit parameter, Q :

$$375 \quad Q = \sum_I \sum_J (E_{ij}/\sigma_{ij})^2 \quad (87)$$

376 where σ_{ij} is the matrix of estimated errors of the data.

377 Solutions using PMF with 2 to 7 factors were explored. The best solution with the optimum
378 number of factors was evaluated carefully using an open source PMF evaluation tool (PET v
379 2.08D, (Ulbrich et al., 2009)) following the procedures described in Zhang et al. (2011).
380 Selection criteria included 1.) variation of the ratio of Q to expected Q_{exp} ($mn-p(m+n)$), the
381 degrees of freedom of the fitted data (Paatero et al., 2002)) after adding an additional factor, 2.)
382 agreement between the reconstructed OA mass concentrations and the measured concentrations,
383 3.) scaled residuals for the different ion fragments included in the dataset and variations of the
384 residual of the solution as a function of time, 4.) agreement between factor time series and time
385 series of external tracers/individual ions, and 5.) examination of factor profiles. The last two are
386 considered to determine the physical meaningfulness of the factors. The PMF solution with
387 factor numbers greater than five and four for winter and summer dataset, respectively, yielded no

388 new distinct and physical meaningful factors. The Q/Q_{exp} and the factors obtained for different
389 FPEAK (from -1 to 1 with a step value of 0.2) values resulted in a small difference in the OA
390 components. Because of the lowest Q/Q_{exp} and because the use of FPEAK values different from
391 0 did not improve the correlations between PMF factors and potentially associated tracers, the
392 five- and four-factors solutions with FPEAK=0 can be well interpreted in winter and summer,
393 respectively. The convergence of the PMF model containing five- and four-factors ~~were~~was
394 examined by running each model from fifteen different starting values (SEEDs 0-30 with a step
395 value of 2). The small variation observed in Q/Q_{exp} and the mass fraction of different factors as
396 SEED changed indicates the solutions were stable. As a result, SEED 0 was chosen for the final
397 solution. The factors were interpreted as hydrocarbon-like OA (HOA), biomass burning OA
398 (BBOA), cooking OA (COA, identified only in the winter campaign), and two oxidized OA
399 (named less-oxygenated (LO-) OOA and more-oxygenated (MO-) OOA). The data treatment,
400 factor selection and interpretation are detailed in the SI. As suggested by El-Sayed et al. (2016),
401 drying of aerosol water may have led to the evaporation of condensed-phase organics. Thus, the
402 resolved mass concentrations of OA factors here are a lower-bound, conservative estimate due to
403 losses of aqueous-SOA in the dryer element.

404 **2.3.3 Estimation of Aerosol Liquid Water Content (LWC)**

405 Aerosol LWC includes water associated with inorganic aerosol and OA, which were
406 calculated using a thermodynamic model and an empirical method, respectively. Inorganic LWC
407 (W_i) in mol L⁻¹ was predicted by ISORROPIA-II in forward mode (Fountoukis and Nenes, 2007).
408 Inputs for ISORROPIA-II include inorganic aerosol mass concentrations (SO_4^{2-} , inorganic NO_3^- ,

409 and NH_4^+) and meteorological parameters (temperature and RH). Calculation empirical of
 410 organic LWC (W_O) follows (Petters and Kreidenweis, 2007; Guo et al., 2015):

$$411 \quad W_O = \frac{m_{org}\rho_w}{\rho_{org}} \frac{\kappa_{org}}{(1/RH)^{-1}} \quad (98)$$

412 where m_{org} is the organic mass concentration ($\mu\text{g m}^{-3}$) and ρ_w is the density of water (1 g
 413 cm^{-3}). The organic density (ρ_{org} , g cm^{-3}) was estimated using an empirical equation based on
 414 elemental ratios (Kuwata et al., 2012; Guo et al., 2015):

$$415 \quad \rho_{org} = 1000 \times \left[\frac{12 + \frac{H}{C} + 16 \times \frac{O}{C}}{7.0 + 5 \times \frac{H}{C} + 4.15 \times \frac{O}{C}} \right] \quad (109)$$

416 The hygroscopicity of SOA generated during chamber studies under sub-saturated regimes
 417 depends on the OA degree of oxidation (Prenni et al., 2007; Jimenez et al., 2009; Petters et al.,
 418 2009; Chang et al., 2010). A simple linear relationship between the OA degree of oxidation
 419 (defined as the fraction of the total signal at m/z 44, f_{44}) and hygroscopicity (κ_{org}) is used
 420 (Duplissy et al., 2011):

$$421 \quad \kappa_{org} = 2.2 \times f_{44} - 0.13 \quad (110)$$

422 The total LWC is then found by summing the water content associated with each mass fraction:

$$423 \quad LWC = W_i + W_O \quad (121)$$

424

425 **3 Results and Discussion**

426 **3.1 Temporal Dependences of Submicron Aerosol Composition**

427 Campaign overview data for winter and summer are shown in Table 1 and Fig. 1. This
 428 includes meteorological parameters (e.g., temperature, RH, radiometer, precipitation, wind

429 direction and speed), trace gases (e.g., CO, SO₂, NO₂, and O₃), and chemically resolved NR-PM₁
430 concentrations.

431 Data indicate that the average concentration of NR-PM₁ during winter campaign was $6.0 \pm$
432 $3.7 \mu\text{g m}^{-3}$, ranging from 0.5 to $14.8 \mu\text{g m}^{-3}$. Mass loadings of NR-PM₁ at this measurement site
433 are relatively smaller than at a site near the HSC in winter 2015 ($10.8 \mu\text{g m}^{-3}$ (Wallace et al.,
434 2018)), perhaps suggesting a weaker industrial influence at the UHSL site.

435 The average concentration of NR-PM₁ during summer was $3.6 \pm 1.7 \mu\text{g m}^{-3}$, ranging from
436 0.3 to $13.7 \mu\text{g m}^{-3}$. For comparison, a summer campaign in 2006 on an elevated building near
437 downtown Houston showed an average NR-PM₁ concentration of approximately $11 \mu\text{g m}^{-3}$
438 (Cleveland et al., 2012). An elevated NR-PM₁ episode was observed from May 28-31 (Fig. 1(J)),
439 with high solar radiation and O_x (O_x = NO₂ + O₃) levels during the daytime, and high RH at
440 night, resulting in OA becoming the largest fractional species, likely due to gas-phase
441 photochemical production of SOA together with the nighttime increase of SOA associated with
442 high RH, lowered boundary layer and cooler temperatures.

443 In winter, OA was the largest component of NR-PM₁, accounting for $38 \pm 13\%$ on average
444 of the total mass, followed by SO₄²⁻ ($23 \pm 11\%$), NO₃⁻ ($23 \pm 11\%$), NH₄⁺ ($15 \pm 5\%$) and Cl⁻ ($1 \pm$
445 0.2%) (Fig. 2). Primary OA (POA=HOA+BBOA+COA) was responsible for $61 \pm 19\%$ of OA
446 mass. Secondary species (SO₄²⁻+NO₃⁻+NH₄⁺+LO-OOA+MO-OOA) accounted for $\sim 76 \pm 21\%$ of
447 NR-PM₁ mass, which is higher than that in winter in Seoul (Kim et al., 2017) and Beijing (Hu et
448 al., 2016).

449 In contrast to winter, OA during the summer campaign constituted on average $47 \pm 18\%$ of
450 NR-PM₁ mass, and SO₄²⁻ was the second largest component ($36 \pm 15\%$), followed by NH₄⁺ ($14 \pm$

451 5%). NO_3^- only accounted for $2 \pm 1\%$ of NR- PM_{10} mass in the summer, and Cl^- contributed $1 \pm$
452 0.5% of NR- PM_{10} mass. The increased planetary boundary layer (PBL) height in summer (Haman
453 et al., 2012) likely contributed to relatively lower trace gas and NR- PM_{10} levels in the summer.
454 Secondary species contributed $\sim 88 \pm 15\%$ of NR- PM_{10} mass, indicating that the relative
455 importance of secondary aerosol formation increased during summer as compared to winter,
456 especially for species such as SO_4^{2-} and MO-OOA.

457 The total OA displayed high values during the nighttime hours in both winter and summer,
458 maintaining a high level until morning rush hour, and then decreasing to a minimum value after
459 9:00 (Fig. 3). The summertime OA presented a small peak at noon, suggesting that
460 photochemical formation of OA played a more important role in summer than in winter.
461 Increasing ambient temperature and PBL height after sunrise causes re-partitioning to the gas
462 phase, likely contributing to the decrease of OA, LO-OOA and ON during daytime.

463 Contributions of PMF factors to wintertime and summertime OA show significant
464 differences. For wintertime OA, on average, BBOA contributed to 26% of OA mass; MO-OOA
465 and COA made the same contributions of 22% to total OA mass. The LO-OOA accounted for 17%
466 of OA mass, followed by HOA (13%). The POA constituted more than half of OA mass (61%),
467 with the remainder of being OOA (39%). In the summer, LO-OOA represented the largest
468 fraction of the OA mass (54% on average), followed by MO-OOA (23%), HOA (15%) and
469 BBOA (8%). In the case of summer, OOA constituted 77% of OA and 36% of total NR- PM_{10}
470 mass, which are almost two times their relative contributions in winter. The time series of mass
471 concentrations of NR- PM_{10} species (Fig. 1) and OA factors (Fig. 4) in summer were relatively
472 stable and repeatable, while they varied dramatically in winter due to the different

473 meteorological conditions.

474

475 **3.2 Seasonal Variation of the Formation of Sulfate and Nitrate**

476 During the summer campaign, the prevailing southerly winds from the Gulf of Mexico carry
477 marine aerosols to Houston (Schulze et al., 2018), resulting in a relatively high fraction of SO_4^{2-}
478 ~~and MSA~~. As shown in Fig. 1(~~gG, jJ~~), the increased contribution of SO_4^{2-} occurred when winds
479 originated from the south at a high speed (e.g., May 16-27), while the contribution of SO_4^{2-}
480 decreased significantly when winds originated from the north (e.g., May 10th and May 13-15).
481 ~~MSA was markedly elevated d~~During periods of southerly winds (~~Fig. S2(F)~~), ~~and~~ O/C and
482 OM/OC were relatively higher (Fig. S2(~~DC~~)). In addition, elevated SO_2 plumes were recorded
483 during periods of southerly winds (Fig. 1(~~gG, hH~~)), potentially as a result of emissions from the
484 Parish coal-fired power plant. In contrast to SO_4^{2-} , the fractional contribution of NO_3^- and OA
485 increased greatly when the winds were not southerly. Primary pollutants such as CO and NO_2 ,
486 were elevated when winds were northerly (Fig. 1(~~hH~~)), accompanied by lower O/C and higher
487 H/C ratios during the corresponding periods (Fig. S2(~~DC~~), e.g., May 1st, 2rd, 10th, 15th).

488 Diurnal patterns of NR- PM_{10} and other species in the winter and summer (Fig. 3) suggest
489 significant seasonal dependence of sources and formation processes of NR- PM_{10} species in
490 Houston. In the case of SO_4^{2-} , the diurnal pattern displayed a daytime peak in both winter and
491 summer, with the peak much more pronounced in summer mid-day. In winter, the f_{SO_4} (mole
492 ratio of $[\text{SO}_4^{2-}]$ to the sum of $[\text{SO}_2]$ and $[\text{SO}_4^{2-}]$) and LWC have concurrent peak values during
493 the night ~~time~~(~~Figure 5~~). However, there is no obvious correlation between f_{SO_4} and LWC in
494 summer, though a moderate correlation ($r = 0.44$) was found in winter. By comparing the diurnal

495 plots of sulfate in winter and summer, it appears that sulfate generated from aqueous chemistry
496 accounted for more mass and a greater fraction of total sulfate production in winter than in
497 summer. These results suggest that SO_4^{2-} formed through aqueous phase chemistry in winter is
498 more prominent than that in summer.

499 The total nitrate concentration was higher in winter than in summer. The $\text{NO}_3^-_{,\text{AN}}$ was very
500 low in summer due to its thermal instability under high temperature, while it was relatively
501 enhanced in winter. According to the NO_x^+ ratio method described in Sec. 2.3.1, the mass
502 fraction of $\text{NO}_3^-_{,\text{AN}}$ in total nitrate was in the range of 65-66% in winter, and in the range of
503 19-39% in summer. The averaged bound concentrations of $\text{NO}_3^-_{,\text{ON}}$ ranged from 0.22-0.34 μg
504 m^{-3} in winter, and 0.05-0.06 $\mu\text{g m}^{-3}$ in summer. The seasonal variation of $\text{NO}_3^-_{,\text{AN}}$ is much
505 stronger than that of $\text{NO}_3^-_{,\text{ON}}$. This is in accordance with previous observations in Atlanta,
506 Georgia and Centreville, Alabama (Xu et al., 2015).

507 The diurnal profiles of $\text{NO}_3^-_{,\text{ON}}$ show that it reached peak value before dawn in both seasons
508 (Fig. 5). However, $\text{NO}_3^-_{,\text{AN}}$ presents a bimodal diurnal profile in both seasons. The $\text{NO}_3^-_{,\text{AN}}$,
509 which increased from late afternoon and peaked at 2:00-4:00, was likely formed through
510 nighttime chemistry from dinitrogen pentoxide (N_2O_5) hydrolysis, as the LWC displayed a trend
511 similar to that of $\text{NO}_3^-_{,\text{AN}}$. This was corroborated by the observation of O_x (>25 ppb), which is
512 needed to form N_2O_5 (via NO_3^\cdot). The second peak observed during morning rush hour was likely
513 formed through photochemical processing of NO_x emitted from vehicles because the traffic flow
514 and O_x level are elevated during morning rush hour. The decreasing trend of $\text{NO}_3^-_{,\text{AN}}$ after 9:00 is
515 presumed to be a result of enhanced PBL height and evaporation.

516 The estimated ON accounted for 4-8% of the total NR- PM_{10} and 9-17% percent of the OA in

517 summer and 12-27% of the total NR-PM₁ and 31-66% percent of the OA in winter, comparable
518 to other studies (Fry et al., 2009; Rollins et al., 2010; Xu et al., 2015; Berkemeier et al., 2016). A
519 proxy for NO₃⁻ production rate is based on the product of the observations of [NO₂] and [O₃]
520 (Rollins et al., 2012), where brackets represent mixing ratios in ppb. The O_x (> 25 ppb) and
521 elevated NO_x observed at night in summer (Fig. 3) resulted in rapid NO₃⁻ formation. Thus, the
522 concurrent enhancement in ON and O₃ times NO₂ occurring during nighttime (Fig. S4)
523 ~~presumably was caused by~~ likely indicates the nocturnal NO₃⁻-initiated oxidation of
524 anthropogenic and biogenic VOCs, with the latter probably larger than the former (Brown et al.,
525 2013). The high N/C ratio of LO-OOA, concurrent peak value in LO-OOA and ON (MW=231 g
526 mol⁻¹) during nighttime hours (Fig. 3), and appreciable correlation of LO-OOA and ON in
527 summer ($r = 0.73$) (Fig. 4) together suggest that particle-phase ON from NO₃⁻-initiated
528 chemistry contributed to nighttime LO-OOA in summer.

529

530 **3.3 Effects of Aqueous-phase and Photochemical Oxidation on OOA Formation**

531 On average, OOA accounted for $39 \pm 19\%$ of OA mass in winter but increased to $77 \pm 16\%$
532 in summer. Note that MO-OOA accounted for more than half of OOA in winter (56%),
533 indicating the more important role of MO-OOA in winter as compared to LO-OOA on a relative
534 basis. In contrast, LO-OOA dominated OOA in summer (70%). The mass spectra of MO-OOA in
535 winter and summer are similar (Fig. 6, $r = 0.84$) as are the extent of oxidation (O/C = 1.10 versus
536 1.07). However, LO-OOA in winter showed a different spectral pattern compared with that in
537 summer. The mass spectrum of LO-OOA in winter was characterized by high m/z 32 (mainly
538 CH₄O⁺) and 46 (mainly CH₂O₂⁺) peaks, resulting in a relatively high O/C (0.89) in winter that

539 suggest LO-OOA in winter was more aged than that in summer ($O/C=0.74$).

540 Sun et al. (2016) reported a unique OOA in ambient air, termed aq-OOA
541 (aqueous-phase-processed SOA), that strongly correlated with particle LWC, sulfate and
542 S-containing ions. As shown in Table 2, by comparing the mass spectra of OOA in this work
543 with aq-OOA, it is found that the mass spectra of MO-OOA in winter in this study presents a
544 much stronger correlation ($r = 0.96$) with aq-OOA, ~~rather than~~ does LO-OOA in winter in this
545 study ($r = 0.75$). Both MO-OOA and LO-OOA in summer highly correlated with aq-OOA. This
546 result indicates that the formation of LO-OOA in summer and MO-OOA in both seasons may
547 involve aqueous-phase chemistry.

548 Assuming that OOA deduced from PMF analysis can be used as a surrogate of SOA (Wood
549 et al., 2010; Xu et al., 2017), the two OOA were used to investigate the formation mechanisms
550 and evolutionary processes of SOA. Previous studies have found SOA correlated well with odd
551 oxygen (O_x) in many cities (Wood et al., 2010; Sun et al., 2011; Hayes et al., 2013; Zhang et al.,
552 2015; Xu et al., 2017) and that SOA formation is significantly impacted by aqueous-phase
553 processing (Lim et al., 2010; Ervens et al., 2011; Xu et al., 2017). The relationships between
554 OOA factors and O_x/LWC were used as the metrics to characterize SOA formation mechanisms
555 associated with photochemistry/aqueous oxidation chemistry (Xu et al., 2017).

556 Fig. 7 (A, B) indicates the LWC frequency distribution. Winter LWC are binned in $5 \mu\text{g m}^{-3}$
557 increments from 0 to $20 \mu\text{g m}^{-3}$. Data in the ranges of 20 to $30 \mu\text{g m}^{-3}$, 30 to $50 \mu\text{g m}^{-3}$, 50 to 80
558 $\mu\text{g m}^{-3}$, and 80 to $120 \mu\text{g m}^{-3}$ are shown as 25, 40, 65 and $100 \mu\text{g m}^{-3}$, respectively. Summer
559 LWC are binned in $2.5 \mu\text{g m}^{-3}$ increments from 0 to $15 \mu\text{g m}^{-3}$. The bins shown as 17.5 and 27.5
560 $\mu\text{g m}^{-3}$ represent data from 15 to $20 \mu\text{g m}^{-3}$ and 20 to $35 \mu\text{g m}^{-3}$. It should be noted that a fit for

561 the binned data likely results in an increase in R^2 compared to the fit for the original data. For
562 example, the correlation coefficient of the fit for the averaged binned wintertime MO-OOA
563 (increased from 0.57 to 0.98 $\mu\text{g m}^{-3}$) versus LWC (increased from 2.5 to 40 $\mu\text{g m}^{-3}$) is 0.55,
564 while it is 0.06 for the original data (Figure 7(I)).

565 The data associated with the artificially created bins in both seasons did not pass the normal
566 test and homogeneity test of variances. The statistical significance of differences between bins
567 was then tested using the Kruskal-Wallis analysis of variance (K-W ANOVA). The differences
568 between winter and summer data of the bins were significant. Thus, the Dunn-Bonferroni test
569 was performed for the *post-hoc* pairwise comparisons. It was found that the difference of all
570 measured variables in different bins shown in Fig. 7 were significant ($p < 0.01$). The results can be
571 found in Tables S6-S7. Fig. 7(C, D) presents a clear positive trend of RH as a function of LWC
572 in both winter and summer which implies an increased potential for aqueous-phase processing at
573 high RH level, enhanced by low wind speed that allows accumulation of pollutants (Fig. 7(E, F)).
574 The patterns of other parameters as LWC increases in winter were different from those in
575 summer.

576 The variation of binned mean OA mass against LWC presents significant seasonal difference
577 (Fig. 7(A, B)). In winter, the OA mass increased when LWC increased from 2.5 to 12.5 $\mu\text{g m}^{-3}$
578 but decreased as the LWC increased further. ~~The LO-OOA mass decreased dramatically when~~
579 ~~LWC > 12.5 $\mu\text{g m}^{-3}$ (RH > 80%, Fig. 7(C)) while MO-OOA continues increasing until LWC > 40~~
580 ~~$\mu\text{g m}^{-3}$. This result indicates that wet removal may dominate under an extremely high RH~~
581 ~~environment coupled with stagnant air (WS < 2 m/s Fig. 7(E)), as the OA concentration~~
582 ~~decreased at extremely high LWC level (Fig. 7(A)).~~ In summer, the OA mass slightly decreased

583 when LWC increased from 1.25 to 6.25 $\mu\text{g m}^{-3}$ but slightly increased when LWC increased
584 further, suggesting the ~~wet removal effect~~production of OA is not as strong as that in winter
585 because of the relatively lower LWC in summer.

586 The winter LO-OOA mass decreased dramatically when $\text{LWC} > 12.5 \mu\text{g m}^{-3}$ ($\text{RH} > 80\%$, Fig.
587 7(C)) while MO-OOA continues increasing until $\text{LWC} > 40 \mu\text{g m}^{-3}$. This result indicates that wet
588 removal may dominate under an extremely high RH environment coupled with stagnant air (WS
589 $< 2 \text{ m/s}$ Fig. 7(E)) or that LO-OOA production decreased at extremely high LWC level (Fig.
590 7(A)). Specifically, ~~On~~ average, LO-OOA (Fig. 7(G, H)) in winter increased from 0.3 to 0.9 μg
591 m^{-3} when LWC increased from 2.5 to 7.5 $\mu\text{g m}^{-3}$ but decreased as the LWC increased further,
592 particularly when $\text{LWC} > 40 \mu\text{g m}^{-3}$. The slope of this decrease was approximately $-0.008 \mu\text{g}$
593 LO-OOA μg^{-1} LWC. Fig. 7(A) shows that 64% of the data points were observed in the situation
594 of low LWC ($< 12.5 \mu\text{g m}^{-3}$, $\text{RH} < 80\%$), when the increase of LO-OOA was ~~more significant than~~
595 ~~that of MO-OOA~~ largest.

596 In contrast, LO-OOA in summer showed a decreasing trend under low LWC level
597 ($\text{LWC} < 6.25 \mu\text{g m}^{-3}$, $\text{RH} < 80\%$) but an increasing trend from approximately 0.77 μm^{-3} to 1.8 μg
598 m^{-3} as LWC increased from 6.25 to 27.5 $\mu\text{g m}^{-3}$, a slope of 0.053 $\mu\text{g LO-OOA } \mu\text{g}^{-1}$ LWC. The
599 relatively high summer LO-OOA under low LWC level was likely more regional, with
600 contributions from possibly transported non-aqueous OOA, as the wind speed in this case was
601 relatively high and RH was low. The ~~formation~~production of LO-OOA under high LWC level
602 ~~was likely~~may have been enhanced by local aqueous-phase heterogeneous chemistry.

603 MO-OOA (~~Fig. 7(I, J)~~) slightly increased during both seasons as LWC increased (Fig. 7(I,
604 J)). In winter, MO-OOA presented a similar increasing trend from 0.57 to 0.98 $\mu\text{g m}^{-3}$ when

605 LWC increased from 2.5 to 40 $\mu\text{g m}^{-3}$ but decreased slightly as the LWC increased further. The
606 slope of this increase was approximately 0.008 $\mu\text{g MO-OOA } \mu\text{g}^{-1} \text{ LWC}$ with correlation
607 coefficient of 0.55. In summer, MO-OOA appears to increase from 0.49 to 0.64 $\mu\text{g m}^{-3}$ when
608 LWC increased from 2.5 to 27.5 $\mu\text{g m}^{-3}$, with slope of 0.005 $\mu\text{g MO-OOA } \mu\text{g}^{-1} \text{ LWC}$ ($R^2=0.34$).
609 In winter, because of the decrease in LO-OOA with LWC, the relative fraction of MO-OOA
610 increases as LWC increases.

611 The mutual effect of aqueous-phase and photochemistry on OOA formation prevents solely
612 evaluating the role of the two processes. Sullivan et al. (2016) reported multiple lines of evidence
613 for local aq-SOA formation observed in the Po Valley, Italy during times of increasing RH,
614 which coincided with dark conditions. Thus, the daytime data were separated to examine the
615 variation of OOA against O_x . The relationship between OOA and aqueous-phase chemistry was
616 investigated further by excluding the daytime data, with the aim of diminishing the instantaneous
617 influence of photochemistry on the data. To do so, nighttime and daytime were based on sunrise
618 and sunset in Houston during the two campaigns
619 (<https://www.timeanddate.com/sun/usa/houston>). On average, the day lengths are 11 h 10 min
620 and 13 h 35 min for the campaigns in February and May, 2014, respectively.

621 ~~The~~ A potential linear relationship between OOA and LWC for the nighttime data was
622 investigated by fitting the data with a locally weighted scatter plot smoothing algorithm
623 (LOWESS, (Cleveland, 1981)). According to the LOWESS curves for the original nighttime data
624 and the resampled data obtained by a bootstrap method (Figs. S14-15), there likely exists a linear
625 relationship between LO-OOA and LWC for data points with LWC less than 20 $\mu\text{g m}^{-3}$ and
626 greater than 6 $\mu\text{g m}^{-3}$ for the winter and summer periods, respectively. As for MO-OOA, such a

627 linear relationship likely exists when LWC is less than 50 and $7 \mu\text{g m}^{-3}$ for the winter and
628 summer periods, respectively.

629 Figure 8 presents the scatter plots of OOA versus LWC during nighttime for the two
630 campaigns. The green dots denote the increasing trend of OOA against LWC. It is found that the
631 increase of wintertime LO-OOA under low LWC level ($<20 \mu\text{g m}^{-3}$) during the night is stronger
632 than that shown in Fig. 7 (G). The nighttime LO-OOA linearly increased from 0.04 to $0.64 \mu\text{g}$
633 m^{-3} when LWC increased from 2.5 to $17.5 \mu\text{g m}^{-3}$, a slope of $0.033 \mu\text{g LO-OOA } \mu\text{g}^{-1} \text{LWC}$. This
634 result indicates that the nighttime ~~increase-production in-of~~ LO-OOA in winter ~~is-may be~~ more
635 likely formed via aqueous-phase chemistry in aerosol liquid water than that in day time. The
636 ~~increase-production~~ of LO-OOA under high LWC level ($\text{LWC} > 6.25 \mu\text{g m}^{-3}$) in summer during
637 nighttime ($0.055 \mu\text{g LO-OOA } \mu\text{g}^{-1} \text{LWC}$) was comparable to the increase rate of whole dataset
638 ($0.053 \mu\text{g LO-OOA } \mu\text{g}^{-1} \text{LWC}$). The nighttime increasing trends of MO-OOA against LWC in
639 both seasons are stronger than those shown in Fig. 7(I, J) with respect to the correlation
640 coefficient values. The slope of nighttime increase of MO-OOA against LWC during the winter
641 campaign was $0.013 \mu\text{g MO-OOA } \mu\text{g}^{-1} \text{LWC}$, which is 1.7 times the slope for the whole dataset
642 (daytime and nighttime). For the summer campaign, the increase of nighttime MO-OOA is 2.2
643 times the rate for the whole dataset.

644 These results suggest that aqueous-phase processing likely has a strong positive impact,
645 particularly at night, on the ~~formation-production~~ of MO-OOA in the two seasons except for
646 instances when LWC exceeds $100 \mu\text{g m}^{-3}$ in winter. It also appears to facilitate the local
647 ~~formation-production~~ of LO-OOA under low LWC level ($<17.5 \mu\text{g m}^{-3}$) in winter and under
648 relatively high LWC level ($>6.25 \mu\text{g m}^{-3}$) in summer.

649 As mentioned previously, ON contributes significantly to summertime LO-OOA, and the
650 concurrent enhancement in ON and LO-OOA during night was associated with elevated RH (Fig.
651 3). A previous study found that the partitioning of organic compounds to the particle phase was
652 significantly increased at elevated RH levels (70%) in an urban area dominated by biogenic
653 emissions in Atlanta (Hennigan et al., 2008). The correlation of ON and LO-OOA in summer
654 nighttime ($r=0.76$) was stronger than that during daytime ($r =0.53$). ~~Thus, we presume that~~
655 ~~aerosol water facilitates the formation of~~This is likely due to the higher ON yields from
656 ~~NO₃⁻-initiated chemistry involving BVOCs during nighttime~~ compared to
657 ~~hydroxyl-radical-initiated chemistry involving BVOCs during daytime, resulting in a good~~
658 ~~relationship of LO-OOA and LWC in summer.~~ Additionally, the concurrent enhancement of the
659 LWC and nitrate functionality from organic nitrate during nighttime demonstrates that the LWC
660 does not inhibit increases in concentration, as might be expected if hydrolysis occurred rapidly.

661 ~~MSA is a secondary product from the oxidation of dimethyl sulfide (Zorn et al., 2008),~~
662 ~~which is a gaseous species emission from marine organisms (Barnes et al., 2006). Thus, MSA is~~
663 ~~found to be abundant in marine/coastal areas and play an important role in the formation of~~
664 ~~marine PM (Gondwe, et al., 2004; Huang et al., 2015; Schulze et al., 2018). The formation of~~
665 ~~MSA is unique to aqueous phase processing and could be used as an indicator of aqueous SOA~~
666 ~~formation (Barnes et al., 2006; Ervens et al., 2011). Recent observations confirmed that MSA~~
667 ~~and associated fragment ions (CH₂O₂⁺ (m/z 46), C₂O₂⁺ (m/z 56) and C₂H₂O₂⁺ (m/z 58), which~~
668 ~~are unique ions of glyoxal and methylglyoxal uptake on SOA (Chhabra et al., 2010)) strongly~~
669 ~~correlated with SOA formed via aqueous phase processing (Ge et al., 2012; Sun et al., 2016). In~~
670 ~~this work, MO-OOA formation was associated with aqueous phase oxidation more strongly than~~

671 ~~LO-OOA in winter, which likely can be further verified by the correlations between~~
672 ~~MO-OOA/LO-OOA and MSA. As shown in Fig. 6, MSA has a relatively higher correlation~~
673 ~~coefficient with MO-OOA ($r=0.45$) compared to LO-OOA ($r=0.30$), though the correlation also~~
674 ~~is influenced by many other factors.~~

675 Fig. 9(A, B) presents the frequency distribution of O_x . Winter O_x are binned in 10 ppb
676 increments from 0 to 60 ppb. The range for summer is 20 to 70 ppb. The data associated with the
677 artificially created O_x bins in both seasons did not pass the normal test and homogeneity test of
678 variances. The K-W ANOVA for winter and summer data of the bins were significant. The
679 Dunn-Bonferroni test for the *post-hoc* pairwise comparisons shows that the difference of
680 measured variables among different bins shown in Fig. 9 were significant (Tables S8-S9). The
681 clear positive relationship between solar radiation and O_x is shown in Fig. 9 (C, D), and the
682 negative relationship between ~~solar radiation~~RH and ~~RH~~ O_x is shown in Fig. 9 (E, F), ~~suggesting~~
683 ~~confirming~~ strong atmospheric photochemical activity associated with high O_x periods.

684 The variations of LO-OOA and MO-OOA showed substantially different patterns with
685 increases of O_x in winter and summer. In winter, LO-OOA and MO-OOA showed comparable
686 increasing trends at low O_x level (<35 ppb), with MO-OOA having a stronger response. The
687 LO-OOA ~~was~~ increased from 0.13 to 0.72 $\mu\text{g m}^{-3}$ when O_x increased from 5 to 35 ppb but
688 decreased as the O_x increased further. The slope of this increase was approximately 0.023 μg
689 LO-OOA $\text{ppb}^{-1} O_x$. MO-OOA increased from 0.13 to 0.88 $\mu\text{g m}^{-3}$ when the O_x increased from 5
690 to 35 ppb, with a slope of 0.027 $\mu\text{g MO-OOA ppb}^{-1} O_x$. This leads to a maximum in the mass
691 fraction of MO-OOA ~~in the mid-as~~ O_x level range and also approached its-at highest observed
692 ~~levels-of observed~~ O_x .

693 In summer, there is a clear decreasing trend of RH with increases of O_x. As discussed
694 previously, the high level of summertime LO-OOA likely was associated with high LWC.
695 Therefore, the high mass fraction of LO-OOA at the lowest O_x level (<20 ppb) associated with
696 the high RH/LWC was likely from aqueous-phase chemistry. After excluding low-O_x data (<20
697 ppb), LO-OOA showed a much stronger response to O_x than did MO-OOA. The summer
698 LO-OOA increased from approximately 0.6 to 1.8 μg m⁻³ when O_x increased from 25 to 65 ppb,
699 a slope of 0.03 μg LO-OOA ppb⁻¹ O_x. This increase was likely in the case of low RH conditions
700 (<80%, Fig. 7 (D)), when aqueous-phase chemistry ~~did not~~ was less likely to promote the
701 formation-production of LO-OOA (Fig. 7 (H)). Summer MO-OOA increased from 0.36 to 0.67
702 μg m⁻³ when O_x increased from 25 to 55 ppb but decreased as the O_x increased further. The slope
703 of this increase was 0.007 μg MO-OOA ppb⁻¹ O_x. Contrary to winter, LO-OOA in summer
704 responded more strongly to increases of O_x than MO-OOA did.

705 The relationship of OOA versus O_x was examined further by excluding nighttime data.
706 According to the LOWESS curves for the original daytime data and the resampled data obtained
707 using a bootstrap method (Figs. S16-17), there likely exists a linear relationship between
708 LO-OOA and O_x when O_x is less than 35 ppb and greater than 20 ppb for the winter and summer
709 period, respectively. As for MO-OOA, the linear relationship likely exists for data points with O_x
710 less than 35 ppb for the winter period, but it is less prominent.

711 Figure 10 presents the scatter plots of daytime OOA versus O_x for the winter and summer
712 campaign. The daytime responses of LO-OOA and MO-OOA to O_x in winter were ~1.5 times
713 that for the whole dataset (Fig. 9 (G, I)), and the increase rate of MO-OOA was higher than that
714 of LO-OOA. In summer, the slope of the daytime increase of LO-OOA was 1.24 times that for

715 the whole campaign (Fig. ~~10-9~~ (H)). These results suggest that the photochemical enhancement
716 of OOA in winter on a per-O_x basis was more prominent than that in summer. For the summer
717 campaign, the formation of LO-OOA ~~was appears to be~~ more strongly linked to photochemistry
718 compared to MO-OOA. ~~At low atmospheric oxidative capacity (O_x<20 ppb), aqueous-phase~~
719 ~~chemistry was likely predominant in the formation of LO-OOA.~~

720 The combined effects of photochemistry and aqueous-phase chemistry on OOA composition
721 during winter and summer are further demonstrated in Fig. 11. The ratio of MO-OOA/LO-OOA
722 in winter showed the highest values on the left-top corner in Fig. 11 (A), suggesting
723 photochemical processing was likely responsible for MO-OOA formation, under low LWC levels
724 (< 10 μg m⁻³). Additionally, data with high MO-OOA/LO-OOA on the right-bottom corner in Fig.
725 11 (A) indicate the important role of aqueous-phase chemistry under low O_x and high LWC
726 levels. Overall, the concentration of MO-OOA in winter increased as O_x/LWC increased,
727 whereas LO-OOA markedly decreased. This result indicates both photochemical and
728 aqueous-phase processing played a more important role in enhancing MO-OOA than LO-OOA
729 in winter. ~~Furthermore, the diurnal patterns of wintertime LO-OOA only presented a peak value~~
730 ~~at night while MO-OOA showed one peak value at night (high LWC) and another one in the~~
731 ~~afternoon (high O_x period) (Fig. 3).~~

732 In summer, data points with low MO-OOA/LO-OOA value on the left-top of Figure 11 (B)
733 illustrated that LO-OOA was enhanced in high-O_x and low-LWC conditions, though the low
734 MO-OOA/LO-OOA values are not confined to just the top left. In case of high LWC level (LWC>
735 6.5 μg m⁻³), MO-OOA/LO-OOA were much lower (on the right of Figure 11 (B), particularly
736 when LWC> 10 μg m⁻³). Although MO-OOA increased with LWC and O_x, the increase of

737 LO-OOA was more significant. The effects of both photochemistry (≥ 25 ppb) and
738 aqueous-phase chemistry ($\geq 6.5 \mu\text{g m}^{-3}$) were more relevant for the formation of LO-OOA than
739 MO-OOA. On average, the mass concentration of LO-OOA was elevated by nearly $1.2 \mu\text{g m}^{-3}$ as
740 a $\sim 20 \mu\text{g}$ change in LWC (increased from $6.25 \mu\text{g m}^{-3}$ to $27.5 \mu\text{g m}^{-3}$, Fig. 7 (H)), which is
741 equivalent to a 40 ppb change in O_x (increased from 25 ppb to 65 ppb, Fig. 9 (H)). This result
742 further suggests that the aqueous-phase chemistry is comparable to photochemistry in processing
743 LO-OOA in summer. ~~The diurnal pattern of summertime LO-OOA displays a peak value at night
744 and a comparable peak value in the afternoon (Fig. 3).~~

745

746 **4 Conclusions**

747 Seasonal characterization of NR-PM₁ collected using HR-ToF-AMS near Houston in 2014
748 demonstrated that the mass loading, diurnal patterns, and important formation pathways of
749 NR-PM₁ vary seasonally. The OA was the largest component of NR-PM₁ mass, on average,
750 accounting for 38% and 47% of the mass loadings in winter and summer, respectively, which is
751 less than that in the north part of Houston, which is influenced by high biogenic emission rates.
752 Nitrate was the second largest component in winter (23%) but accounted for only 2% of NR-PM₁
753 mass in summer; SO_4^{2-} was the second largest component in winter (23%) and summer (36%),
754 respectively. ON, on average accounted for 31-66 and 9-17 % of OA during winter and summer
755 campaign, respectively. The summertime ON correlated very well with LO-OOA and
756 concurrently peaked at nighttime. It is likely that ON from NO_3^- -initiated oxidation of BVOC
757 in the forested northeastern Houston contributed greatly to nighttime LO-OOA in summer and
758 that LWC did not inhibit resulting concentration growth.

759 Contributions of factors to wintertime and summertime OA show distinct differences. For
760 wintertime OA, on average, BBOA contributed 26% of OA mass, and MO-OOA and COA made
761 the same contribution of 22% to total OA mass. LO-OOA accounted for 17% of OA mass,
762 followed by HOA (13%). In the summer, LO-OOA represented the largest fraction of the OA
763 mass, 54% on average. The second largest contributor was MO-OOA (23%). Together, POA
764 constituted more than half of OA mass (61%) in winter, while it accounted for 23% of OA mass
765 in summer, highlighting the enhanced impact of primary emissions on OA level during
766 wintertime. Secondary aerosols account for ~76% and 88% of NR-PM₁ mass in winter and
767 summer, respectively, indicating NR-PM₁ mass was likely driven mostly by secondary aerosol
768 formation.

769 The two proxies of SOA (LO-OOA and MO-OOA) presented seasonal differences in their
770 spectral patterns, oxidation degrees and contributions to SOA. MO-OOA showed a higher
771 contribution to SOA than LO-OOA in winter (56% vs. 44%). In contrast, LO-OOA dominated
772 SOA in summer (70%). Our results indicate that both photochemical and aqueous-phase
773 chemistry, as suggested by relationships to O_x and LWC, played important roles in the formation
774 of MO-OOA and LO-OOA. Aqueous-phase processing likely has strong positive impact on the
775 formation of MO-OOA in the two seasons, especially in winter. The relationships between
776 MO-OOA and LWC were 0.008 and 0.005 μg MO-OOA μg⁻¹ LWC during winter and summer,
777 respectively. Wet removal or decreased formation rates likely limits MO-OOA when LWC
778 exceeds 100 μg m⁻³ in winter. The relative importance of aqueous-phase chemistry versus
779 photochemistry in processing LO-OOA was dependent on RH. Aqueous-phase processing likely
780 potentially facilitated the local formation of wintertime LO-OOA at low LWC level (<17.5 μg

781 m^{-3} , $\text{RH}<80\%$), with a stronger dependence ($0.033 \mu\text{g LO-OOA } \mu\text{g}^{-1} \text{ LWC}$) than MO-OOA. In
782 summer, the formation of LO-OOA ~~was~~may have been enhanced by aqueous-phase processing
783 at relatively high LWC level ($>6.25 \mu\text{g m}^{-3}$, $\text{RH}>80\%$) with a slope of $0.053 \mu\text{g LO-OOA } \mu\text{g}^{-1}$
784 LWC, while LO-OOA was likely transported non-aqueous regional OOA when $\text{LWC} < 6.25 \mu\text{g}$
785 m^{-3} . These increases of OOA in ~~response~~relation to LWC were greatly enhanced during
786 nighttime. Aqueous-phase chemistry also ~~was~~appears predominant important in the formation of
787 summertime LO-OOA at low atmospheric oxidative capacity ($\text{O}_x < 20 \text{ ppb}$). In general,
788 summertime LO-OOA showed a much stronger response to O_x than did MO-OOA, with a slope
789 of $0.030 \mu\text{g LO-OOA ppb}^{-1} \text{ O}_x$. LO-OOA in summer was elevated by nearly $1.2 \mu\text{g m}^{-3}$ as a ~ 20
790 μg change in LWC, which is equivalent to a 40 ppb change in O_x .

791

792 **Acknowledgments**

793 The authors would like to acknowledge Yele Sun (Institute of Atmospheric Physics, Chinese
794 Academy of Sciences) for providing the aq-OOA mass spectra, and Qiao Zhu (Peking University
795 Shenzhen Graduate School) for assistance in the calculation of organic nitrates and PMF analysis.
796 The scholarships provided by China Scholarship Council to Qili Dai and Xiaohui Bi are
797 gratefully acknowledged. Support of the Houston Endowment in development and deployment
798 of the MAQL also is gratefully acknowledged. Datasets are available by contacting the
799 corresponding author.

800

801 *Author contribution.* Qili Dai performed the data analysis and wrote the manuscript. Robert J.
802 Griffin and Yinchang Feng assisted heavily with manuscript development and editing. Henry W.
803 Wallace, Alexander A.T. Bui, James H. Flynn, and Barry L. Lefer contributed to data collection
804 during the field campaigns. Benjamin C. Schulze, Henry W. Wallace, Alexander A.T. Bui and
805 Nancy P. Sanchez contributed with data analysis. Xiaohui Bi, Benjamin C. Schulze, Alexander
806 A.T. Bui, Fangzhou Guo, Nancy P. Sanchez, and James H. Flynn provided helpful comments
807 and edits.

808

809 *Competing interests.* The authors declare that they have no conflict of interest.

810

811 **References**

- 812 Allen, D. T., and Fraser, M.: An overview of the Gulf Coast Aerosol Research and
813 Characterization Study: The Houston Fine Particulate Matter Supersite, *J. Air Waste*
814 *Manage.*, 56, 456-466, <http://doi.org/10.1080/10473289.2006.10464514>, 2006.
- 815 Atkinson, D. B., Massoli, P., O'Neill, N. T., Quinn, P. K., Brooks, S. D., and Lefer, B.:
816 Comparison of in situ and columnar aerosol spectral measurements during
817 TexAQS-GoMACCS 2006: testing parameterizations for estimating aerosol fine mode
818 properties, *Atmos. Chem. Phys.*, 10, 51-61, <http://doi.org/10.5194/acp-10-51-2010>, 2010.
- 819 Ayres, B. R., Allen, H. M., Draper, D. C., Brown, S. S., Wild, R. J., Jimenez, J. L., Day, D. A.,
820 Campuzano-Jost, P., Hu, W., de Gouw, J., Koss, A., Cohen, R. C., Duffey, K. C., Romer, P.,
821 Baumann, K., Edgerton, E., Takahama, S., Thornton, J. A., Lee, B. H., Lopez-Hilfiker, F. D.,
822 Mohr, C., Wennberg, P. O., Nguyen, T. B., Teng, A., Goldstein, A. H., Olson, K., and Fry, J.
823 L.: Organic nitrate aerosol formation via NO₃ + biogenic volatile organic compounds in the
824 southeastern United States, *Atmos. Chem. Phys.*, 15, 13377-13392,
825 <http://doi.org/10.5194/acp-15-13377-2015>, 2015.
- 826 Bahreini, R., Ervens, B., Middlebrook, A. M., Warneke, C., de Gouw, J. A., DeCarlo, P. F.,
827 Jimenez, J. L., Brock, C. A., Neuman, J. A., Ryerson, T. B., Stark, H., Atlas, E., Brioude, J.,

828 Fried, A., Holloway, J. S., Peischl, J., Richter, D., Walega, J., Weibring, P., Wollny, A. G.,
829 and Fehsenfeld, F. C.: Organic aerosol formation in urban and industrial plumes near
830 Houston and Dallas, Texas, *J. Geophys. Res.*, 114, D00f16,
831 <http://doi.org/10.1029/2008jd011493>, 2009.

~~832 Barnes, I., Hjorth, J., and Mihalopoulos, N.: Dimethyl sulfide and dimethyl sulfoxide and their~~
~~833 oxidation in the atmosphere, *Chem. Rev.*, 106, 940–975, <http://doi.org/10.1021/cr020529>,~~
~~834 2006.~~

835 Bates, T. S., Quinn, P. K., Coffman, D., Schulz, K., Covert, D. S., Johnson, J. E., Williams, E. J.,
836 Lerner, B. M., Angevine, W. M., Tucker, S. C., Brewer, W. A., and Stohl, A.: Boundary layer
837 aerosol chemistry during TexAQS/GoMACCS 2006: Insights into aerosol sources and
838 transformation processes, *J. Geophys. Res.*, 113, D00f01,
839 <http://doi.org/10.1029/2008jd010023>, 2008.

840 Bean, J. K., Faxon, C. B., Leong, Y. J., Wallace, H. W., Cevik, B. K., Ortiz, S., Canagaratna, M.
841 R., Usenko, S., Sheesley, R. J., Griffin, R. J., and Hildebrandt, L.: Composition and sources
842 of particulate matter measured near Houston, TX; Anthropogenic-biogenic interactions,
843 *Atmos.*, 7, 73, <https://doi.org/10.3390/atmos7050073>, 2016

844 Berkemeier, T., Ammann, M., Mentel, T. F., Poschl, U., and Shiraiwa, M.: Organic Nitrate
845 Contribution to New Particle Formation and Growth in Secondary Organic Aerosols from
846 alpha-Pinene Ozonolysis, *Environ. Sci. Technol.*, 50, 6334–6342,
847 <http://doi.org/10.1021/acs.est.6b00961>, 2016.

848 Boyd, C. M., Sanchez, J., Xu, L., Eugene, A. J., Nah, T., Tuet, W. Y., Guzman, M. I., and Ng, N.
849 L.: Secondary Organic Aerosol (SOA) formation from the β -pinene CNO₃ system: effect of
850 humidity and peroxy radical fate, *Atmos. Chem. Phys.*, 15, 7497–7522,
851 [doi:10.5194/acp-15-7497-2015](https://doi.org/10.5194/acp-15-7497-2015), 2015.

852 Brown, S. S., Dube, W. P., Bahreini, R., Middlebrook, A. M., Brock, C. A., Warneke, C., de
853 Gouw, J. A., Washenfelder, R. A., Atlas, E., Peischl, J., Ryerson, T. B., Holloway, J. S.,
854 Schwarz, J. P., Spackman, R., Trainer, M., Parrish, D. D., Fehshenfeld, F. C., and
855 Ravishankara, A. R.: Biogenic VOC oxidation and organic aerosol formation in an urban
856 nocturnal boundary layer: aircraft vertical profiles in Houston, TX, *Atmos. Chem. Phys.*, 13,
857 11317–11337, <http://doi.org/10.5194/acp-13-11317-2013>, 2013.

858 Bruns, E. A., Perraud, V., Zelenyuk, A., Ezell, M. J., Johnson, S. N., Yu, Y., Imre, D.,
859 Finlayson-Pitts, B. J., and Alexander, M. L.: Comparison of FTIR and Particle Mass
860 Spectrometry for the Measurement of Particulate Organic Nitrates, *Environ. Sci. Technol.*,

861 44, 1056–1061, 2010.

862 Canagaratna, M. R., Jayne, J. T., Jimenez, J. L., Allan, J. D., Alfarra, M. R., Zhang, Q., Onasch, T.
863 B., Drewnick, F., Coe, H., Middlebrook, A., Delia, A., Williams, L. R., Trimborn, A. M.,
864 Northway, M. J., DeCarlo, P. F., Kolb, C. E., Davidovits, P., and Worsnop, D. R.: Chemical
865 and microphysical characterization of ambient aerosols with the aerodyne aerosol mass
866 spectrometer, *Mass Spectrom. Rev.*, 26, 185-222, <http://doi.org/10.1002/mas.20115>, 2007.

867 Canagaratna, M. R., Jimenez, J. L., Kroll, J. H., Chen, Q., Kessler, S. H., Massoli, P.,
868 Hildebrandt Ruiz, L., Fortner, E., Williams, L. R., Wilson, K. R., Surratt, J. D., Donahue, N.
869 M., Jayne, J. T., and Worsnop, D. R.: Elemental ratio measurements of organic compounds
870 using aerosol mass spectrometry: characterization, improved calibration, and implications,
871 *Atmos. Chem. Phys.*, 15, 253-272, <http://doi.org/10.5194/acp-15-253-2015>, 2015.

872 Chang, R. Y. W., Slowik, J. G., Shantz, N. C., Vlasenko, A., Liggio, J., Sjostedt, S. J., Leaitch, W.
873 R., and Abbatt, J. P. D.: The hygroscopicity parameter (κ) of ambient organic aerosol at
874 a field site subject to biogenic and anthropogenic influences: relationship to degree of
875 aerosol oxidation, *Atmos. Chem. Phys.*, 10, 5047-5064,
876 <http://doi.org/10.5194/acp-10-5047-2010>, 2010.

877 ~~Chhabra, P. S., Flagan, R. C., and Seinfeld, J. H.: Elemental analysis of chamber organic aerosol~~
878 ~~using an aerodyne high-resolution aerosol mass spectrometer, *Atmos. Chem. Phys.*, 10,~~
879 ~~4111-4131, <http://doi.org/10.5194/acp-10-4111-2010>, 2010.~~

880 Cleveland, M. J., Ziemba, L. D., Griffin, R. J., Dibb, J. E., Anderson, C. H., Lefer, B., and
881 Rappengluck, B.: Characterization of urban aerosol using aerosol mass spectrometry and
882 proton nuclear magnetic resonance spectroscopy, *Atmos. Environ.*, 54, 511-518,
883 <http://doi.org/10.1016/j.atmosenv.2012.02.074>, 2012.

884 Cleveland, W. S. (1981) LOWESS: A program for smoothing scatterplots by robust locally
885 weighted regression. *Am. Stat.*, 35, 54.

886 Crippa, M., El Haddad, I., Slowik, J. G., DeCarlo, P. F., Mohr, C., Heringa, M. F., Chirico, R.,
887 Marchand, N., Sciare, J., Baltensperger, U., and Prevot, A. S. H.: Identification of marine
888 and continental aerosol sources in Paris using high resolution aerosol mass spectrometry, *J.*
889 *Geophys. Res.*, 118, 1950-1963, <http://doi.org/10.1002/jgrd.50151>, 2013.

890 DeCarlo, P. F., Kimmel, J. R., Trimborn, A., Northway, M. J., Jayne, J. T., Aiken, A. C., Gonin,
891 M., Fuhrer, K., Horvath, T., Docherty, K. S., Worsnop, D. R., and Jimenez, J. L.:
892 Field-deployable, high-resolution, time-of-flight aerosol mass spectrometer, *Anal. Chem.*, 78,
893 8281-8289, <http://doi.org/10.1021/ac061249n>, 2006.

- 894 Duplissy, J., DeCarlo, P. F., Dommen, J., Alfarra, M. R., Metzger, A., Barmapadimos, I., Prevot, A.
895 S. H., Weingartner, E., Tritscher, T., Gysel, M., Aiken, A. C., Jimenez, J. L., Canagaratna, M.
896 R., Worsnop, D. R., Collins, D. R., Tomlinson, J., and Baltensperger, U.: Relating
897 hygroscopicity and composition of organic aerosol particulate matter, *Atmos. Chem. Phys.*,
898 11, 1155-1165, <http://doi.org/10.5194/acp-11-1155-2011>, 2011.
- 899 El-Sayed, M. M. H., Amenumey, D., and Hennigan, C. J.: Drying-Induced Evaporation of
900 Secondary Organic Aerosol during Summer, *Environ Sci Technol*, 50, 3626-3633,
901 10.1021/acs.est.5b06002, 2016.
- 902 Ervens, B., Turpin, B. J., and Weber, R. J.: Secondary organic aerosol formation in cloud droplets
903 and aqueous particles (aqSOA): a review of laboratory, field and model studies, *Atmos.*
904 *Chem. Phys.*, 11, 11069-11102, <http://doi.org/10.5194/acp-11-11069-2011>, 2011.
- 905 Farmer, D. K., Matsunaga, A., Docherty, K. S., Surratt, J. D., Seinfeld, J. H., Ziemann, P. J., and
906 Jimenez, J. L.: Response of an aerosol mass spectrometer to organonitrates and
907 organosulfates and implications for atmospheric chemistry, *P. Natl. Acad. Sci. USA*, 107,
908 6670-6675, <http://doi.org/10.1073/pnas.0912340107>, 2010.
- 909 Fountoukis, C., and Nenes, A.: ISORROPIA II: a computationally efficient thermodynamic
910 equilibrium model for $K^+-Ca^{2+}-Mg^{2+}-NH_4^+-Na^+-SO_4^{2-}-NO_3^- -Cl^- -H_2O$ aerosols,
911 *Atmos. Chem. Phys.*, 7, 4639-4659, <http://doi.org/10.5194/acp-7-4639-2007>, 2007.
- 912 Fry, J. L., Kiendler-Scharr, A., Rollins, A. W., Wooldridge, P. J., Brown, S. S., Fuchs, H., Dube,
913 W., Mensah, A., dal Maso, M., Tillmann, R., Dorn, H. P., Brauers, T., and Cohen, R. C.:
914 Organic nitrate and secondary organic aerosol yield from NO_3 oxidation of beta-pinene
915 evaluated using a gas-phase kinetics/aerosol partitioning model, *Atmos. Chem. Phys.*, 9,
916 1431-1449, <http://doi.org/10.5194/acp-9-1431-2009>, 2009.
- 917 Fry, J. L., Draper, D. C., Zarzana, K. J., Campuzano-Jost, P., Day, D. A., Jimenez, J. L., Brown, S.
918 S., Cohen, R. C., Kaser, L., Hansel, A., Cappellin, L., Karl, T., Roux, A. H., Turnipseed, A.,
919 Cantrell, C., Lefer, B. L., and Grossberg, N.: Observations of gas- and aerosol-phase organic
920 nitrates at BEACHON-RoMBAS 2011, *Atmos. Chem. Phys.*, 13, 8585-8605,
921 <http://doi.org/10.5194/acp-13-8585-2013>, 2013.
- ~~922 Ge, X., Zhang, Q., Sun, Y., Ruehl, C. R., and Setyan, A.: Effect of aqueous phase processing on~~
~~923 aerosol chemistry and size distributions in Fresno, California, during wintertime, *Environ.*~~
~~924 *Chem.*, 9, 221, <http://doi.org/10.1071/en11168>, 2012.~~
- ~~925 Gondwe, M., Krol, M., Klaassen, W., Gieskes, W., and de Baar, H.: Comparison of modeled~~
~~926 versus measured MSA:nss SO_4 ratios: A global analysis, *Global Biogeochem. Cy.*, 18,~~

- 927 <http://doi.org/10.1029/2003GB002144>, 2004.
- 928 Grantz, D. A., Garner, J. H. B., and Johnson, D. W.: Ecological effects of particulate matter,
929 *Environ. Int.*, 29, 213-239, [http://doi.org/10.1016/S0160-4120\(02\)00181-2](http://doi.org/10.1016/S0160-4120(02)00181-2), 2003.
- 930 Guo, H., Xu, L., Bougiatioti, A., Cerully, K. M., Capps, S. L., Hite, J. R., Carlton, A. G., Lee, S.
931 H., Bergin, M. H., Ng, N. L., Nenes, A., and Weber, R. J.: Fine-particle water and pH in the
932 southeastern United States, *Atmos. Chem. Phys.*, 15, 5211-5228,
933 <http://doi.org/10.5194/acp-15-5211-2015>, 2015.
- 934 Haman, C. L., Lefer, B., and Morris, G. A.: Seasonal Variability in the Diurnal Evolution of the
935 Boundary Layer in a Near-Coastal Urban Environment, *J. Atmos. Ocean Tech.*, 29,
936 697-710, , <http://doi.org/10.1175/Jtech-D-11-00114.1>, 2012.
- 937 Hayes, P. L., Ortega, A. M., Cubison, M. J., Froyd, K. D., Zhao, Y., Cliff, S. S., Hu, W. W.,
938 Toohey, D. W., Flynn, J. H., Lefer, B. L., Grossberg, N., Alvarez, S., Rappenglueck, B.,
939 Taylor, J. W., Allan, J. D., Holloway, J. S., Gilman, J. B., Kuster, W. C., De Gouw, J. A.,
940 Massoli, P., Zhang, X., Liu, J., Weber, R. J., Corrigan, A. L., Russell, L. M., Isaacman, G.,
941 Worton, D. R., Kreisberg, N. M., Goldstein, A. H., Thalman, R., Waxman, E. M., Volkamer,
942 R., Lin, Y. H., Surratt, J. D., Kleindienst, E., Offenberg, J. H., Dusanter, S., Griffith, S.,
943 Stevens, P. S., Brioude, J., Angevine, W. M., and Jimenez, J. L.: Organic aerosol
944 composition and sources in Pasadena, California, during the 2010 CalNex campaign, *J.*
945 *Geophys. Res.*, 118, 9233-9257, <http://doi.org/10.1002/jgrd.50530>, 2013.
- 946 Hennigan, C. J., Bergin, M. H., Dibb, J. E., and Weber, R. J.: Enhanced secondary organic
947 aerosol formation due to water uptake by fine particles, *Geophys. Res. Lett.*, 35, L18801,
948 <http://doi.org/10.1029/2008gl035046>, 2008.
- 949 Hu, W. W., Campuzano-Jost, P., Palm, B. B., Day, D. A., Ortega, A. M., Hayes, P. L., Krechmer,
950 J. E., Chen, Q., Kuwata, M., Liu, Y. J., de Sa, S. S., McKinney, K., Martin, S. T., Hu, M.,
951 Budisulistiorini, S. H., Riva, M., Surratt, J. D., St Clair, J. M., Isaacman-Van Wertz, G., Yee,
952 L. D., Goldstein, A. H., Carbone, S., Brito, J., Artaxo, P., de Gouw, J. A., Koss, A., Wisthaler,
953 A., Mikoviny, T., Karl, T., Kaser, L., Jud, W., Hansel, A., Docherty, K. S., Alexander, M. L.,
954 Robinson, N. H., Coe, H., Allan, J. D., Canagaratna, M. R., Paulot, F., and Jimenez, J. L.:
955 Characterization of a real-time tracer for isoprene epoxydiols-derived secondary organic
956 aerosol (IEPOX-SOA) from aerosol mass spectrometer measurements, *Atmos. Chem. Phys.*,
957 15, 11807-11833, <http://doi.org/10.5194/acp-15-11807-2015>, 2015.
- 958 Hu, W. W., Hu, M., Hu, W., Jimenez, J. L., Yuan, B., Chen, W. T., Wang, M., Wu, Y. S., Chen, C.,
959 Wang, Z. B., Peng, J. F., Zeng, L. M., and Shao, M.: Chemical composition, sources, and

960 aging process of submicron aerosols in Beijing: Contrast between summer and winter, J.
961 Geophys. Res., 121, 1955-1977, <http://doi.org/10.1002/2015jd024020>, 2016.

962 ~~Huang, D. D., Li, Y. J., Lee, B. P., and Chan, C. K.: Analysis of Organic Sulfur Compounds in~~
963 ~~Atmospheric Aerosols at the HKUST Supersite in Hong Kong using HR-ToF-AMS, Environ.~~
964 ~~Sci. Technol., 49, 3672-3679, <http://doi.org/10.1021/es5056269>, 2015.~~

965 Jimenez, J. L., Canagaratna, M. R., Donahue, N. M., Prevot, A. S. H., Zhang, Q., Kroll, J. H.,
966 DeCarlo, P. F., Allan, J. D., Coe, H., Ng, N. L., Aiken, A. C., Docherty, K. S., Ulbrich, I. M.,
967 Grieshop, A. P., Robinson, A. L., Duplissy, J., Smith, J. D., Wilson, K. R., Lanz, V. A.,
968 Hueglin, C., Sun, Y. L., Tian, J., Laaksonen, A., Raatikainen, T., Rautiainen, J., Vaattovaara,
969 P., Ehn, M., Kulmala, M., Tomlinson, J. M., Collins, D. R., Cubison, M. J., Dunlea, E. J.,
970 Huffman, J. A., Onasch, T. B., Alfarra, M. R., Williams, P. I., Bower, K., Kondo, Y.,
971 Schneider, J., Drewnick, F., Borrmann, S., Weimer, S., Demerjian, K., Salcedo, D., Cottrell,
972 L., Griffin, R., Takami, A., Miyoshi, T., Hatakeyama, S., Shimono, A., Sun, J. Y., Zhang, Y.
973 M., Dzepina, K., Kimmel, J. R., Sueper, D., Jayne, J. T., Herndon, S. C., Trimborn, A. M.,
974 Williams, L. R., Wood, E. C., Middlebrook, A. M., Kolb, C. E., Baltensperger, U., and
975 Worsnop, D. R.: Evolution of Organic Aerosols in the Atmosphere, *Science*, 326, 1525-1529,
976 <http://doi.org/10.1126/science.1180353>, 2009.

977 Kim, H., Zhang, Q., Bae, G. N., Kim, J. Y., and Lee, S. B.: Sources and atmospheric processing
978 of winter aerosols in Seoul, Korea: insights from real-time measurements using a
979 high-resolution aerosol mass spectrometer, *Atmos. Chem. Phys.*, 17, 2009-2033,
980 <http://doi.org/10.5194/acp-17-2009-2017>, 2017.

981 Kota, S. H., Park, C., Hale, M. C., Werner, N. D., Schade, G. W., and Ying, Q.: Estimation of
982 VOC emission factors from flux measurements using a receptor model and footprint analysis,
983 *Atmos Environ*, 82, 24-35, [10.1016/j.atmosenv.2013.09.052](https://doi.org/10.1016/j.atmosenv.2013.09.052), 2014.

984 Kuwata, M., Zorn, S. R., and Martin, S. T.: Using Elemental Ratios to Predict the Density of
985 Organic Material Composed of Carbon, Hydrogen, and Oxygen, *Environ. Sci. Technol.*, 46,
986 787-794, <http://doi.org/10.1021/es202525q>, 2012.

987 Leong, Y. J., Sanchez, N. P., Wallace, H. W., Cevik, B. K., Hernandez, C. S., Han, Y., Flynn, J. H.,
988 Massoli, P., Floerchinger, C., Fortner, E. C., Herndon, S., Bean, J. K., Hildebrandt Ruiz, L.,
989 Jeon, W., Choi, Y., Lefer, B., and Griffin, R. J.: Overview of surface measurements and
990 spatial characterization of submicrometer particulate matter during the DISCOVER-AQ
991 2013 campaign in Houston, TX, *J. Air Waste Manage.*, 67, 854-872,
992 <http://doi.org/10.1080/10962247.2017.1296502>, 2017.

993 Leuchner, M., and Rappengluck, B.: VOC source-receptor relationships in Houston during
994 TexAQS-II, *Atmos Environ*, 44, 4056-4067, [10.1016/j.atmosenv.2009.02.029](https://doi.org/10.1016/j.atmosenv.2009.02.029), 2010.

995 Li, J. Y., Cleveland, M., Ziemba, L. D., Griffin, R. J., Barsanti, K. C., Pankow, J. F., and Ying, Q.:
996 Modeling regional secondary organic aerosol using the Master Chemical Mechanism, *Atmos.*
997 *Environ.*, 102, 52-61, <http://doi.org/10.1016/j.atmosenv.2014.11.054>, 2015.

998 Lim, Y. B., Tan, Y., Perri, M. J., Seitzinger, S. P., and Turpin, B. J.: Aqueous chemistry and its
999 role in secondary organic aerosol (SOA) formation, *Atmos. Chem. Phys.*, 10, 10521-10539,
1000 <http://doi.org/10.5194/acp-10-10521-2010>, 2010.

1001 Liu, J. B., Rhland, K. M., Chen, J. H., Xu, Y. Y., Chen, S. Q., Chen, Q. M., Huang, W., Xu, Q. H.,
1002 Chen, F. H., and Smol, J. P.: Aerosol-weakened summer monsoons decrease lake fertilization
1003 on the Chinese Loess Plateau, *Nat. Clim. Change*, 7, 190-194, <http://10.1038/Nclimate3220>,
1004 2017.

1005 Mao, J. Q., Ren, X. R., Chen, S. A., Brune, W. H., Chen, Z., Martinez, M., Harder, H., Lefter, B.,
1006 Rappengluck, B., Flynn, J., and Leuchner, M.: Atmospheric oxidation capacity in the
1007 summer of Houston 2006: Comparison with summer measurements in other metropolitan
1008 studies, *Atmos. Environ.*, 44, 4107-4115, <http://doi.org/10.1016/j.atmosenv.2009.01.013>,
1009 2010.

1010 McKeen, S., Grell, G., Peckham, S., Wilczak, J., Djalalova, I., Hsie, E. Y., Frost, G., Peischl, J.,
1011 Schwarz, J., Spackman, R., Holloway, J., de Gouw, J., Warneke, C., Gong, W., Bouchet, V.,
1012 Gaudreault, S., Racine, J., McHenry, J., McQueen, J., Lee, P., Tang, Y., Carmichael, G. R.,
1013 and Mathur, R.: An evaluation of real-time air quality forecasts and their urban emissions
1014 over eastern Texas during the summer of 2006 Second Texas Air Quality Study field study, *J.*
1015 *Geophys. Res.*, 114, D00f11, <http://doi.org/10.1029/2008JD011697>, 2009.

1016 Middlebrook, A. M., Bahreini, R., Jimenez, J. L., and Canagaratna, M. R.: Evaluation of
1017 Composition-Dependent Collection Efficiencies for the Aerodyne Aerosol Mass
1018 Spectrometer using Field Data, *Aerosol Sci. Tech.*, 46, 258-271,
1019 <http://doi.org/10.1080/02786826.2011.620041>, 2012.

1020 Olaguer, E. P., Kolb, C. E., Lefter, B., Rappenglueck, B., Zhang, R. Y., and Pinto, J. P.: Overview
1021 of the SHARP campaign: Motivation, design, and major outcomes, *J. Geophys. Res.*, 119,
1022 2597-2610, <http://doi.org/10.1002/2013jd019730>, 2014.

1023 Paatero, P., Hopke, P. K., Song, X. H., and Ramadan, Z.: Understanding and controlling rotations
1024 in factor analytic models, *Chemometr. Intell. Lab*, 60, 253-264,
1025 [http://doi.org/10.1016/S0169-7439\(01\)00200-3](http://doi.org/10.1016/S0169-7439(01)00200-3), 2002.

1026 Paatero, P., and Tapper, U.: Positive matrix factorization: A non-negative factor model with
1027 optimal utilization of error estimates of data values, *Environmetrics*, 5, 111-126,
1028 <https://doi.org/10.1002/env.3170050203>, 1994.

1029 Parrish, D. D., Allen, D. T., Bates, T. S., Estes, M., Fehsenfeld, F. C., Feingold, G., Ferrare, R.,
1030 Hardesty, R. M., Meagher, J. F., Nielsen-Gammon, J. W., Pierce, R. B., Ryerson, T. B.,
1031 Seinfeld, J. H., and Williams, E. J.: Overview of the Second Texas Air Quality Study
1032 (TexAQS II) and the Gulf of Mexico Atmospheric Composition and Climate Study
1033 (GoMACCS), *J. Geophys. Res.*, 114, D00f13, <http://doi.org/10.1029/2009jd011842>, 2009.

1034 Petters, M. D., and Kreidenweis, S. M.: A single parameter representation of hygroscopic growth
1035 and cloud condensation nucleus activity, *Atmos. Chem. Phys.*, 7, 1961-1971, ,
1036 <http://doi.org/10.5194/acp-7-1961-2007>, 2007.

1037 Petters, M. D., Wex, H., Carrico, C. M., Hallbauer, E., Massling, A., McMeeking, G. R., Poulain,
1038 L., Wu, Z., Kreidenweis, S. M., and Stratmann, F.: Towards closing the gap between
1039 hygroscopic growth and activation for secondary organic aerosol - Part 2: Theoretical
1040 approaches, *Atmos. Chem. Phys.*, 9, 3999-4009, <http://doi.org/10.5194/acp-9-3999-2009>,
1041 2009.

1042 Prenni, A. J., Petters, M. D., Kreidenweis, S. M., DeMott, P. J., and Ziemann, P. J.: Cloud droplet
1043 activation of secondary organic aerosol, *J. Geophys. Res.*, 112, D10223,
1044 <http://doi.org/10.1029/2006jd007963>, 2007.

1045 Racherla, P. N., and Adams, P. J.: Sensitivity of global tropospheric ozone and fine particulate
1046 matter concentrations to climate change, *J. Geophys. Res.*, 111,
1047 <https://doi.org/10.1029/2005JD006939>, 2006.

1048 Rollins, A. W., Smith, J. D., Wilson, K. R., and Cohen, R. C.: Real Time In Situ Detection of
1049 Organic Nitrates in Atmospheric Aerosols, *Environ. Sci. Technol.*, 44, 5540-5545,
1050 <http://doi.org/10.1021/es100926x>, 2010.

1051 Rollins, A. W., Browne, E. C., Min, K. E., Pusede, S. E., Wooldridge, P. J., Gentner, D. R.,
1052 Goldstein, A. H., Liu, S., Day, D. A., Russell, L. M., and Cohen, R. C.: Evidence for NOx
1053 Control over Nighttime SOA Formation, *Science*, 337, 1210-1212,
1054 <http://doi.org/10.1126/science.1221520>, 2012.

1055 Russell, L. M., Takahama, S., Liu, S., Hawkins, L. N., Covert, D. S., Quinn, P. K., and Bates, T.
1056 S.: Oxygenated fraction and mass of organic aerosol from direct emission and atmospheric
1057 processing measured on the R/V Ronald Brown during TEXAQS/GoMACCS 2006, *J.*
1058 *Geophys. Res.*, 114, D00F05, <http://doi.org/10.1029/2008JD011275>, 2009.

1059 Schulze, B. C., Wallace, H. W., Bui, A. T., Flynn, J. H., Erickson, M. H., Alvarez, S., Dai, Q.,
1060 Usenko, S., Sheesley, R. J., and Griffin, R. J.: The impacts of regional shipping emissions on
1061 the chemical characteristics of coastal submicron aerosols near Houston, TX, *Atmos. Chem.*
1062 *Phys.*, 18, 14217-14241, <http://doi.org/10.5194/acp-18-14217-2018>, 2018.

1063 Setyan, A., Zhang, Q., Merkel, M., Knighton, W. B., Sun, Y., Song, C., Shilling, J. E., Onasch, T.
1064 B., Herndon, S. C., Worsnop, D. R., Fast, J. D., Zaveri, R. A., Berg, L. K., Wiedensohler, A.,
1065 Flowers, B. A., Dubey, M. K., and Subramanian, R.: Characterization of submicron particles
1066 influenced by mixed biogenic and anthropogenic emissions using high-resolution aerosol
1067 mass spectrometry: results from CARES, *Atmos. Chem. Phys.*, 12, 8131-8156,
1068 <http://doi.org/10.5194/acp-12-8131-2012>, 2012.

1069 Sullivan, A. P., Hodas, N., Turpin, B. J., Skog, K., Keutsch, F. N., Gilardoni, S., Paglione, M.,
1070 Rinaldi, M., Decesari, S., Facchini, M. C., Poulain, L., Herrmann, H., Wiedensohler, A.,
1071 Nemitz, E., Twigg, M. M., and Collett Jr, J. L.: Evidence for ambient dark aqueous SOA
1072 formation in the Po Valley, Italy, *Atmos. Chem. Phys.*, 16, 8095-8108,
1073 <http://doi.org/10.5194/acp-16-8095-2016>, 2016.

1074 Sun, Y. L., Zhang, Q., Schwab, J. J., Demerjian, K. L., Chen, W. N., Bae, M. S., Hung, H. M.,
1075 Hogrefe, O., Frank, B., Rattigan, O. V., and Lin, Y. C.: Characterization of the sources and
1076 processes of organic and inorganic aerosols in New York city with a high-resolution
1077 time-of-flight aerosol mass spectrometer, *Atmos. Chem. Phys.*, 11, 1581-1602,
1078 <https://doi.org/10.5194/acp-11-1581-2011>, 2011.

1079 Sun, Y. L., Du, W., Fu, P. Q., Wang, Q. Q., Li, J., Ge, X. L., Zhang, Q., Zhu, C. M., Ren, L. J.,
1080 Xu, W. Q., Zhao, J., Han, T. T., Worsnop, D. R., and Wang, Z. F.: Primary and secondary
1081 aerosols in Beijing in winter: sources, variations and processes, *Atmos. Chem. Phys.*, 16,
1082 8309-8329, <http://doi.org/10.5194/acp-16-8309-2016>, 2016.

1083 Surratt, J. D., Gomez-Gonzalez, Y., Chan, A. W. H., Vermeulen, R., Shahgholi, M., Kleindienst,
1084 T. E., Edney, E. O., Offenberg, J. H., Lewandowski, M., Jaoui, M., Maenhaut, W., Claeys,
1085 M., Flagan, R. C., and Seinfeld, J. H.: Organosulfate formation in biogenic secondary
1086 organic aerosol, *J. Phys. Chem. A*, 112, 8345-8378, <http://doi.org/10.1021/jp802310p>, 2008.

1087 Tai, A. P. K., Mickley, L. J., and Jacob, D. J.: Correlations between fine particulate matter
1088 (PM_{2.5}) and meteorological variables in the United States: Implications for the sensitivity of
1089 PM_{2.5} to climate change, *Atmos. Environ.*, 44, 3976-3984,
1090 <http://10.1016/j.atmosenv.2010.06.060>, 2010.

1091 Ulbrich, I. M., Canagaratna, M. R., Zhang, Q., Worsnop, D. R., and Jimenez, J. L.: Interpretation

1092 of organic components from Positive Matrix Factorization of aerosol mass spectrometric
1093 data, *Atmos. Chem. Phys.*, 9, 2891-2918, <https://doi.org/10.5194/acp-9-2891-2009>, 2009.

1094 Wallace, H. W., Sanchez, N. P., Flynn, J. H., Erickson, M. H., Lefer, B. L., and Griffin, R. J.:
1095 Source apportionment of particulate matter and trace gases near a major refinery near the
1096 Houston Ship Channel, *Atmos. Environ.*, 173, 16-29,
1097 <https://doi.org/10.1016/j.atmosenv.2017.10.049>, 2018.

1098 Watson, J. G.: Visibility: Science and regulation, *J. Air Waste Manage.*, 52, 628-713,
1099 <http://doi.org/10.1080/10473289.2002.10470813>, 2002.

1100 Wood, E. C., Canagaratna, M. R., Herndon, S. C., Onasch, T. B., Kolb, C. E., Worsnop, D. R.,
1101 Kroll, J. H., Knighton, W. B., Seila, R., Zavala, M., Molina, L. T., DeCarlo, P. F., Jimenez, J.
1102 L., Weinheimer, A. J., Knapp, D. J., Jobson, B. T., Stutz, J., Kuster, W. C., and Williams, E.
1103 J.: Investigation of the correlation between odd oxygen and secondary organic aerosol in
1104 Mexico City and Houston, *Atmos. Chem. Phys.*, 10, 8947-8968,
1105 <http://doi.org/10.5194/acp-10-8947-2010>, 2010.

1106 Xu, L., Suresh, S., Guo, H., Weber, R. J., and Ng, N. L.: Aerosol characterization over the
1107 southeastern United States using high-resolution aerosol mass spectrometry: spatial and
1108 seasonal variation of aerosol composition and sources with a focus on organic nitrates,
1109 *Atmos. Chem. Phys.*, 15, 7307-7336, <http://doi.org/10.5194/acp-15-7307-2015>, 2015.

1110 Xu, W. Q., Han, T. T., Du, W., Wang, Q. Q., Chen, C., Zhao, J., Zhang, Y. J., Li, J., Fu, P. Q.,
1111 Wang, Z. F., Worsnop, D. R., and Sun, Y. L.: Effects of Aqueous-Phase and Photochemical
1112 Processing on Secondary Organic Aerosol Formation and Evolution in Beijing, China,
1113 *Environ. Sci. Technol.*, 51, 762-770, <http://doi.org/10.1021/acs.est.6b04498>, 2017.

1114 Ying, Q., Li, J. Y., and Kota, S. H.: Significant Contributions of Isoprene to Summertime
1115 Secondary Organic Aerosol in Eastern United States, *Environ. Sci. Technol.*, 49, 7834-7842,
1116 <http://doi.org/10.1021/acs.est.5b02514>, 2015.

1117 Zhang, Q., Jimenez, J. L., Canagaratna, M. R., Ulbrich, I. M., Ng, N. L., Worsnop, D. R., and
1118 Sun, Y. L.: Understanding atmospheric organic aerosols via factor analysis of aerosol mass
1119 spectrometry: a review, *Anal. Bioanal. Chem.*, 401, 3045-3067,
1120 <https://doi.org/10.1007/s00216-011-5355-y>, 2011.

1121 Zhang, Q. J., Beekmann, M., Freney, E., Sellegri, K., Pichon, J. M., Schwarzenboeck, A.,
1122 Colomb, A., Bourriane, T., Michoud, V., and Borbon, A.: Formation of secondary organic
1123 aerosol in the Paris pollution plume and its impact on surrounding regions, *Atmos. Chem.*
1124 *Phys.*, 15, 13973-13992, <http://doi.org/10.5194/acp-15-13973-2015>, 2015.

1125 Zhu, Q., He, L. Y., Huang, X. F., Cao, L. M., Gong, Z. H., Wang, C., Zhuang, X., and Hu, M.:
1126 Atmospheric aerosol compositions and sources at two national background sites in northern
1127 and southern China, *Atmos. Chem. Phys.*, 16, 10283-10297,
1128 <http://doi.org/10.5194/acp-16-10283-2016>, 2016.

1129 ~~Zorn, S. R., Drewnick, F., Schott, M., Hoffmann, T., and Borrmann, S.: Characterization of the~~
1130 ~~South Atlantic marine boundary layer aerosol using an aerodyne aerosol mass spectrometer,~~
1131 ~~*Atmos. Chem. Phys.*, 8, 4711-4728, <http://doi.org/10.5194/acp-8-4711-2008>, 2008.~~

1132

1133 **Table 1** Statistics of meteorological parameters, gas-phase pollutants, NR-PM₁ species, and PMF OA
 1134 factors for the winter and summer campaigns at UHSL.

	Variables	Season	Ave. value ± 1 SD	Minimum value	Maximum value
Meteorological parameters	Temp (°C)	Winter	9.3 ± 6.0	0.7	25.9
		Summer	23.6 ± 3.8	12.2	33.1
	RH (%)	Winter	76 ± 18	23	99
		Summer	72 ± 19	21	98
	WS (m s ⁻¹)	Winter	2.1 ± 1.4	6.8×10 ⁻³	9.4
		Summer	2.1 ± 1.2	9.0×10 ⁻³	6.7
Radiometer (W m ⁻²)	Winter	0.6 ± 0.9	0.02	3.6	
	Summer	1.1 ± 1.3	0.02	4.6	
Gas-phase pollutants (ppb)	O ₃	Winter	23.0 ± 12.6	0.12	53.0
		Summer	34.9 ± 15.3	0.02	75.9
	CO	Winter	238.7 ± 71.9	98.5	621.1
		Summer	168.3 ± 75.5	103.6	1110.2
	SO ₂	Winter	1.0 ± 1.9	5.7×10 ⁻³	29.5
		Summer	0.7 ± 1.7	2.8×10 ⁻³	30.9
	NO	Winter	4.3 ± 6.4	2.0×10 ⁻³	74.9
		Summer	1.3 ± 4.6	0.01	68.1
	NO ₂	Winter	12.5 ± 9.7	0.8	101.2
		Summer	4.6 ± 6.4	0.2	44.4
NO _y	Winter	22.9 ± 19.6	2.8	210.9	
	Summer	8.6 ± 11.9	1.3	123.9	
NR-PM ₁ species (µg m ⁻³)	OA	Winter	2.3 ± 1.4	0.42	9.4
		Summer	1.7 ± 1.4	0.27	12.3
	Sulfate	Winter	1.4 ± 0.8	0.05	3.4
		Summer	1.3 ± 0.6	0.02	5.6
	Nitrate	Winter	1.4 ± 1.4	0.02	6.9
		Summer	0.08 ± 0.1	0.01	0.9
	Ammonium	Winter	0.9 ± 0.6	BDL ^a	2.8
		Summer	0.5 ± 0.2	0.02	1.8
	Chloride	Winter	0.06 ± 0.09	BDL	1.1
		Summer	0.02 ± 0.02	BDL	0.5
OA factors (µg m ⁻³)	HOA	Winter	0.3 ± 0.4	0 ^b	8.6
		Summer	0.2 ± 0.5	0	10.9
	BBOA	Winter	0.6 ± 0.6	0	3.7
		Summer	0.1 ± 0.3	0	5.4
	COA	Winter	0.5 ± 0.5	0	4.8
	LO-OOA	Winter	0.4 ± 0.5	0	2.1
		Summer	0.7 ± 0.9	0	6.7
	MO-OOA	Winter	0.5 ± 0.3	0	1.8
Summer		0.3 ± 0.2	0	1.6	

1135 ^aBDL: below detection limit; ^bStatistically determined factor concentrations with values below 1.0×10⁻³ are listed as
 1136 0.

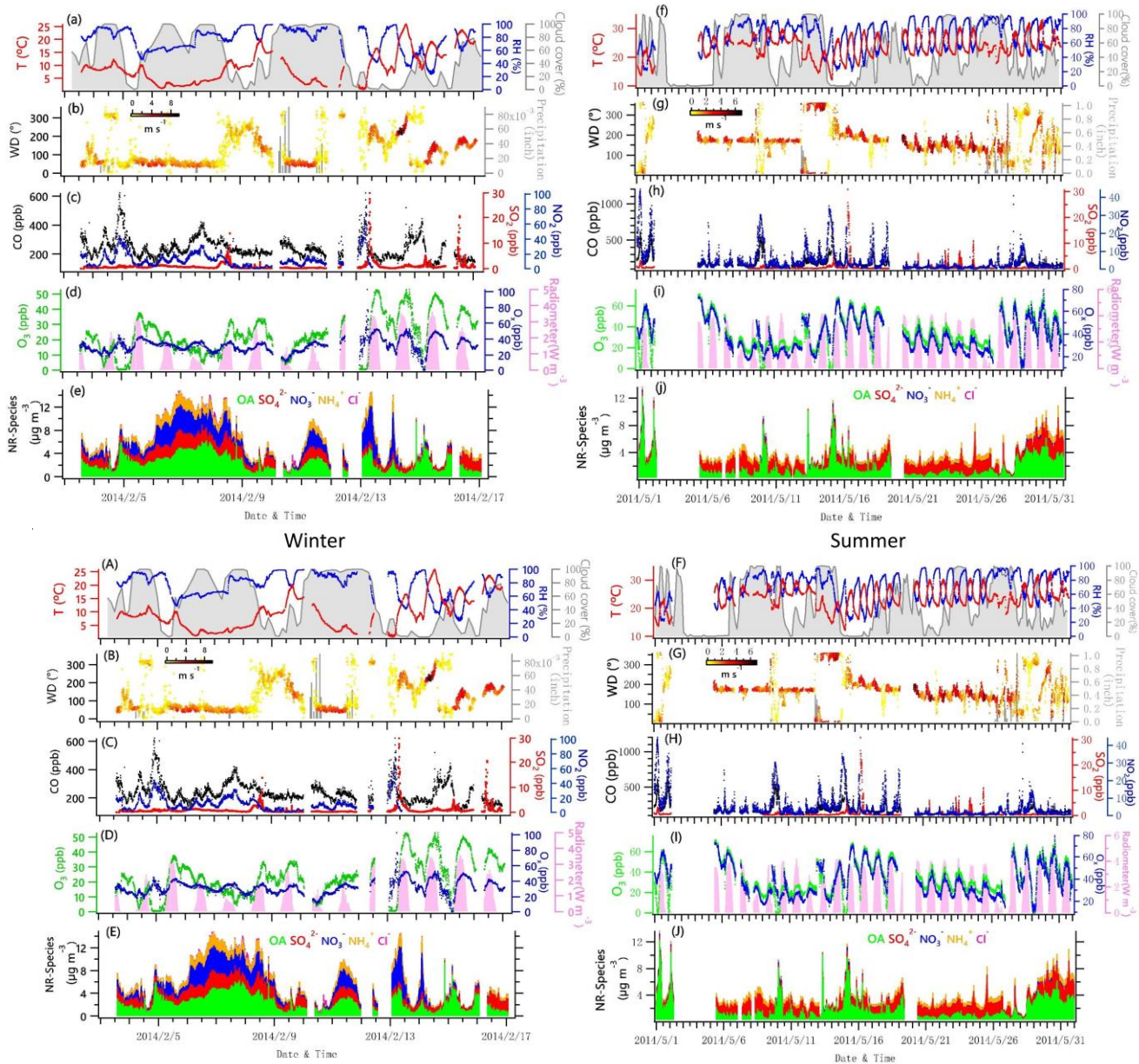
1138 **Table 2** Correlation (*r*) of OOA mass spectra with previously published spectra database.
 1139 (<http://cires1.colorado.edu/jimenez-group/HRAMSsd/>)

Factor	Winter		Summer		Reference
	MO-OOA	LO-OOA	MO-OOA	LO-OOA	
aq-OOA ^a	0.96	0.75	0.96	0.95	Sun et al., 2016
MO-OOA	0.85	0.87	0.89	0.77	Setyan et al., 2012
MO-OOA	0.98	0.92	0.98	0.60	Hu et al., 2015
LV-OOA	0.97	0.91	0.98	0.62	Crippa et al., 2013
SV-OOA	0.65	0.70	0.70	0.78	Crippa et al., 2013
LO-OOAI, Biogenic-origin	0.83	0.84	0.86	0.76	Hu et al., 2015
LO-OOAII, Anthropogenic-origin	0.78	0.80	0.82	0.74	Hu et al., 2015

1140 ^aaq-OOA is an aqueous-phase-processed SOA reported by Sun et al. (2016); LV=less ~~volatility~~volatile;

1141 SV=semi-volatile.

1142

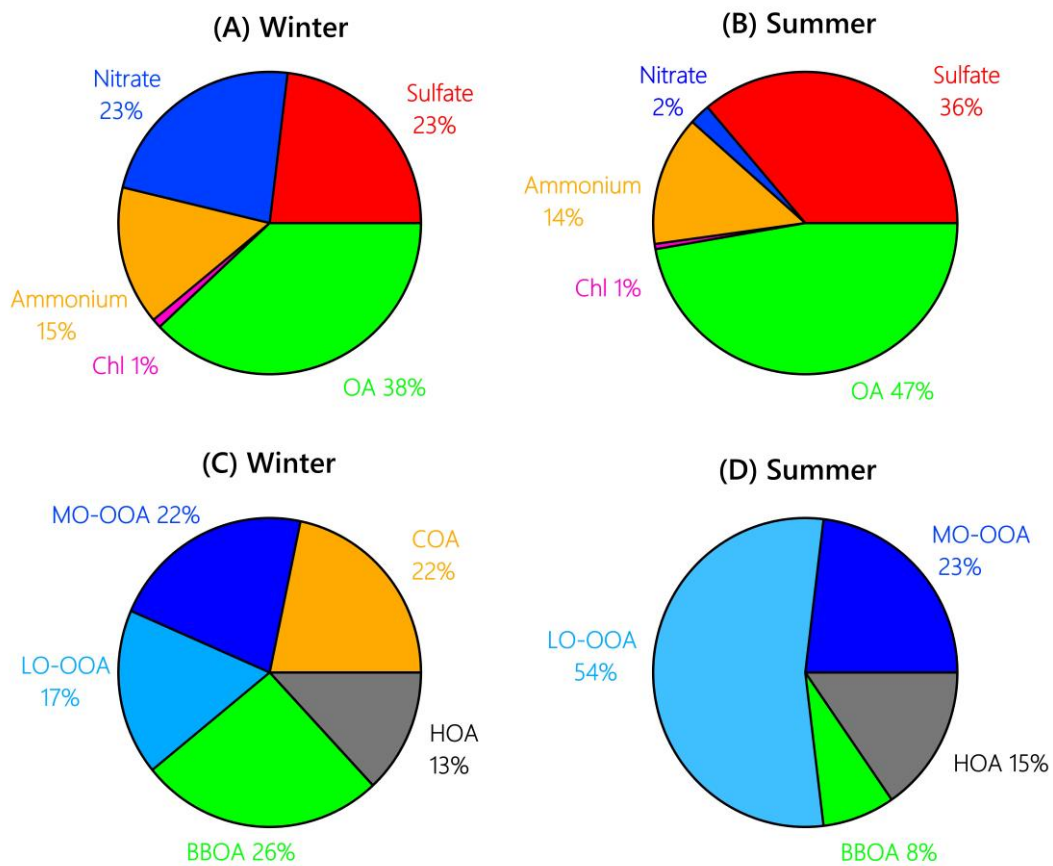


1144

1145

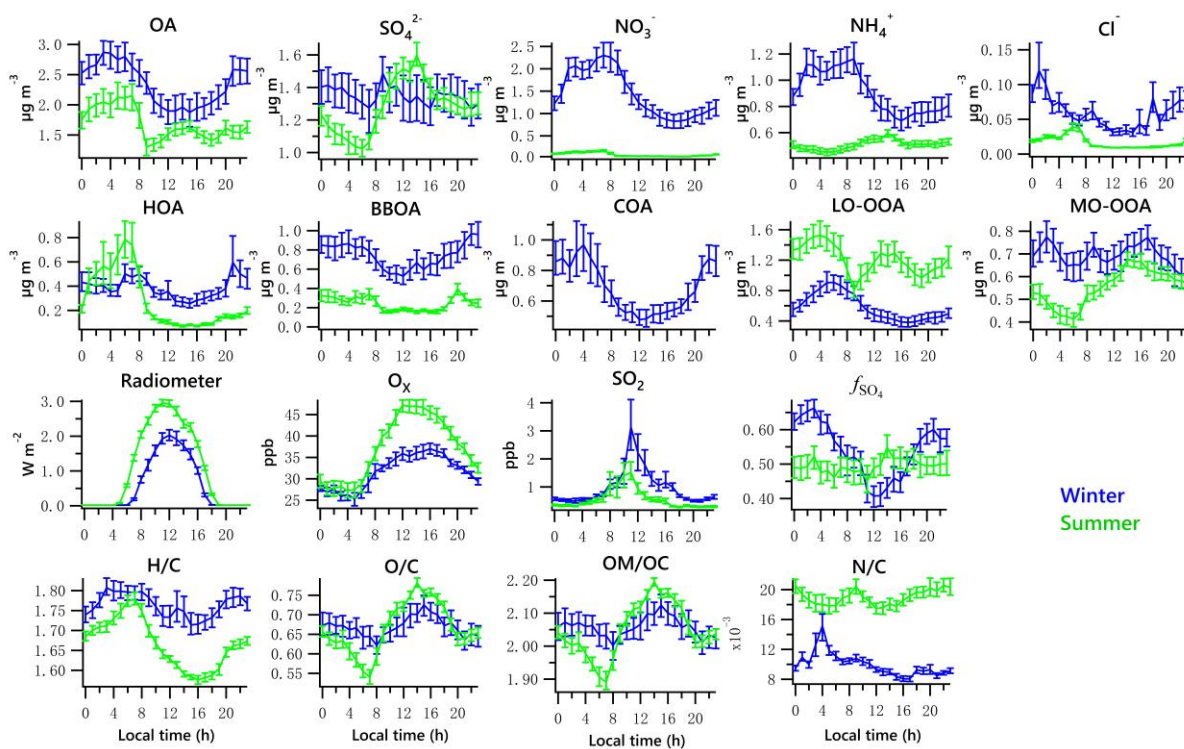
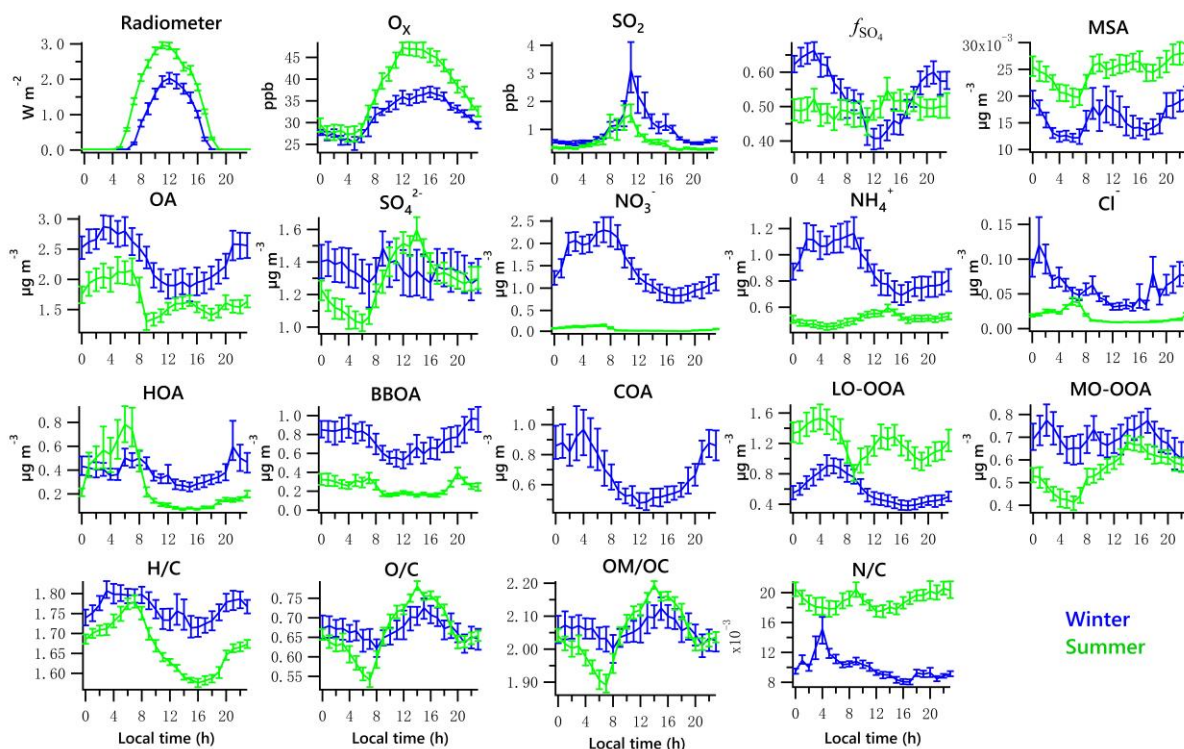
1146 **Figure 1.** Time series of data collected at UHSL in Houston during the sampling periods in
 1147 winter and summer 2014. Time series of 5-min average campaign data for **(aA, fF)** ambient
 1148 temperature (T), relative humidity (RH) and total cloud cover (% with 3 hours interval); **(bB,**
 1149 **gG)** precipitation and wind direction (WD), with colors showing different wind speeds (WS);
 1150 **(cC, hH)** CO, SO₂ and NO₂; **(dD, iI)** O₃, O_x (NO₂+O₃) and solar radiometer; **(eE, jJ)** NR-PM₁
 1151 species, including OA, NO₃⁻, SO₄²⁻, NH₄⁺, and Cl⁻.

1152



1153
 1154 **Figure 2.** Average composition of NR-PM₁ species and OA factors during the winter (**A, C**) and
 1155 summer campaign (**B, D**) at UHSL.

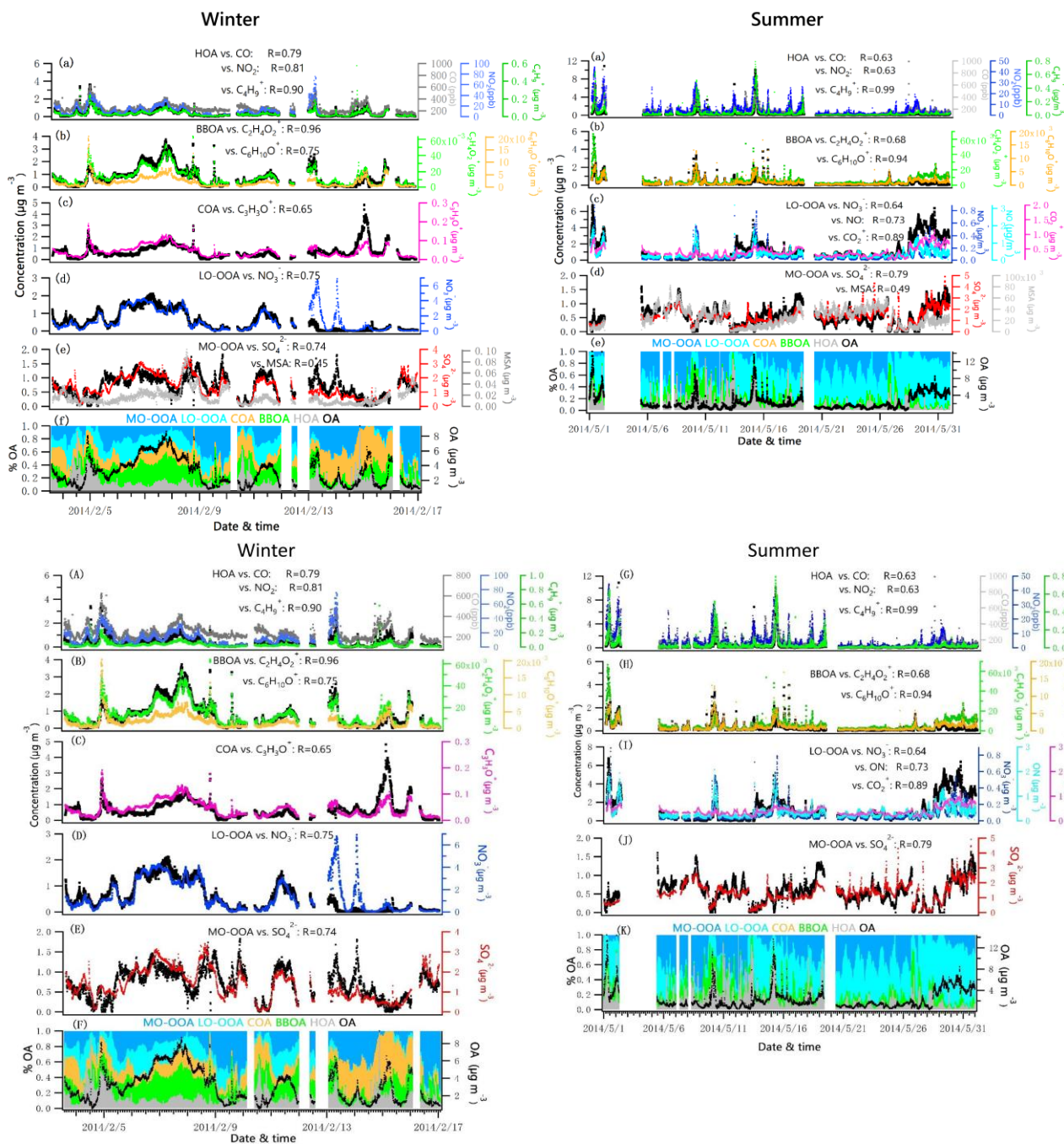
1156
 1157



1158

1159

1160 **Figure 3.** Diurnal profiles of radiometer, O_x , SO_2 , f_{SO_4} , MSA, each of the five NR-PM₁ species
 1161 (OrgOA, SO_4^{2-} , NO_3^- , NH_4^+ and Cl^-), PMF-resolved factors (HOA, BBOA, COA, LO-OOA and
 1162 MO-OOA), radiometer, O_x , SO_2 , f_{SO_4} , and elemental ratios (H/C, O/C, OM/OC and N/C). Lines
 1163 denote the mean value, and bars represent the 5/95 percent confidence interval in the mean (blue
 1164 for winter, green for summer).

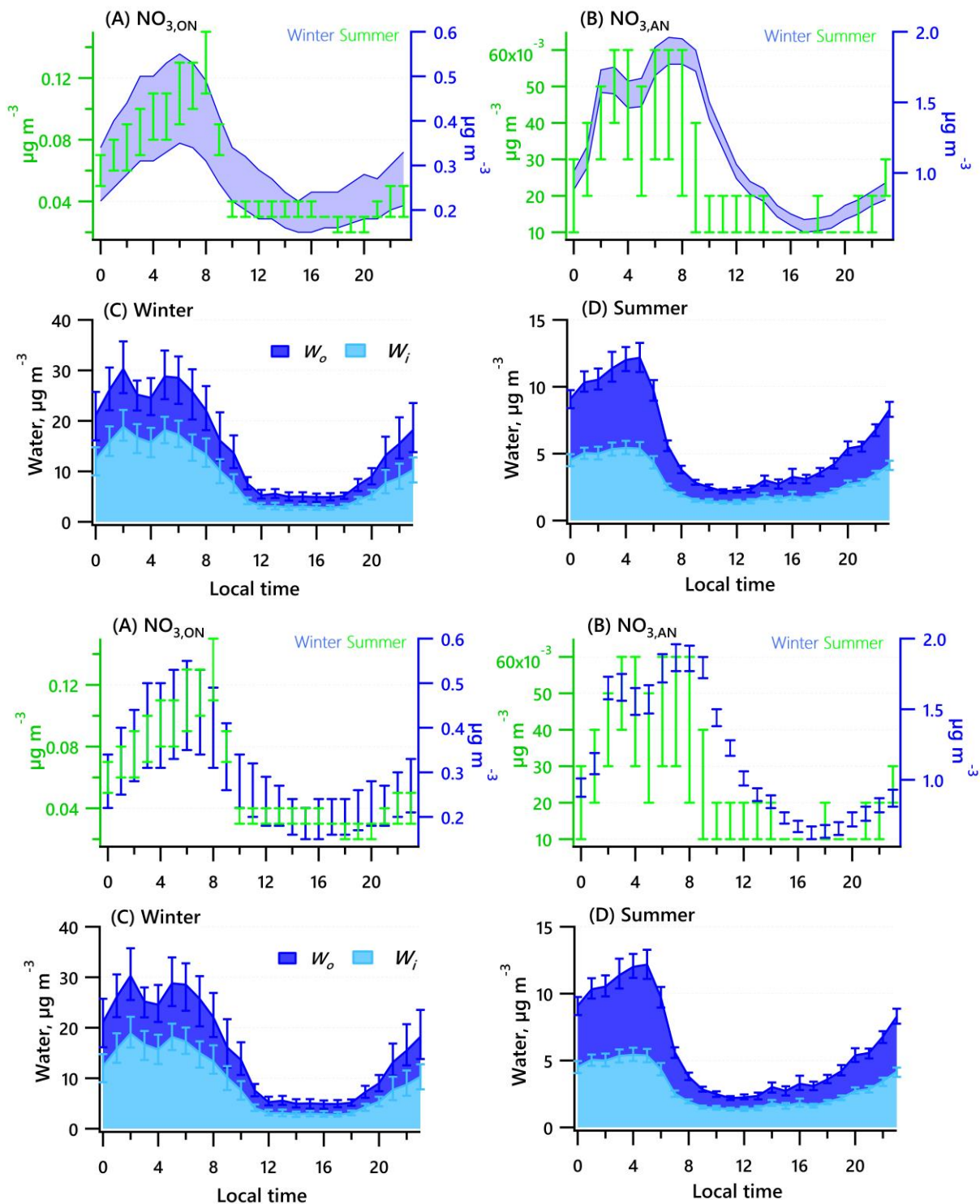


1166

1167

1168 **Figure 4.** Time series of each OA factor and associated correlated species for the winter and
 1169 summer campaign at UHSL.

1170

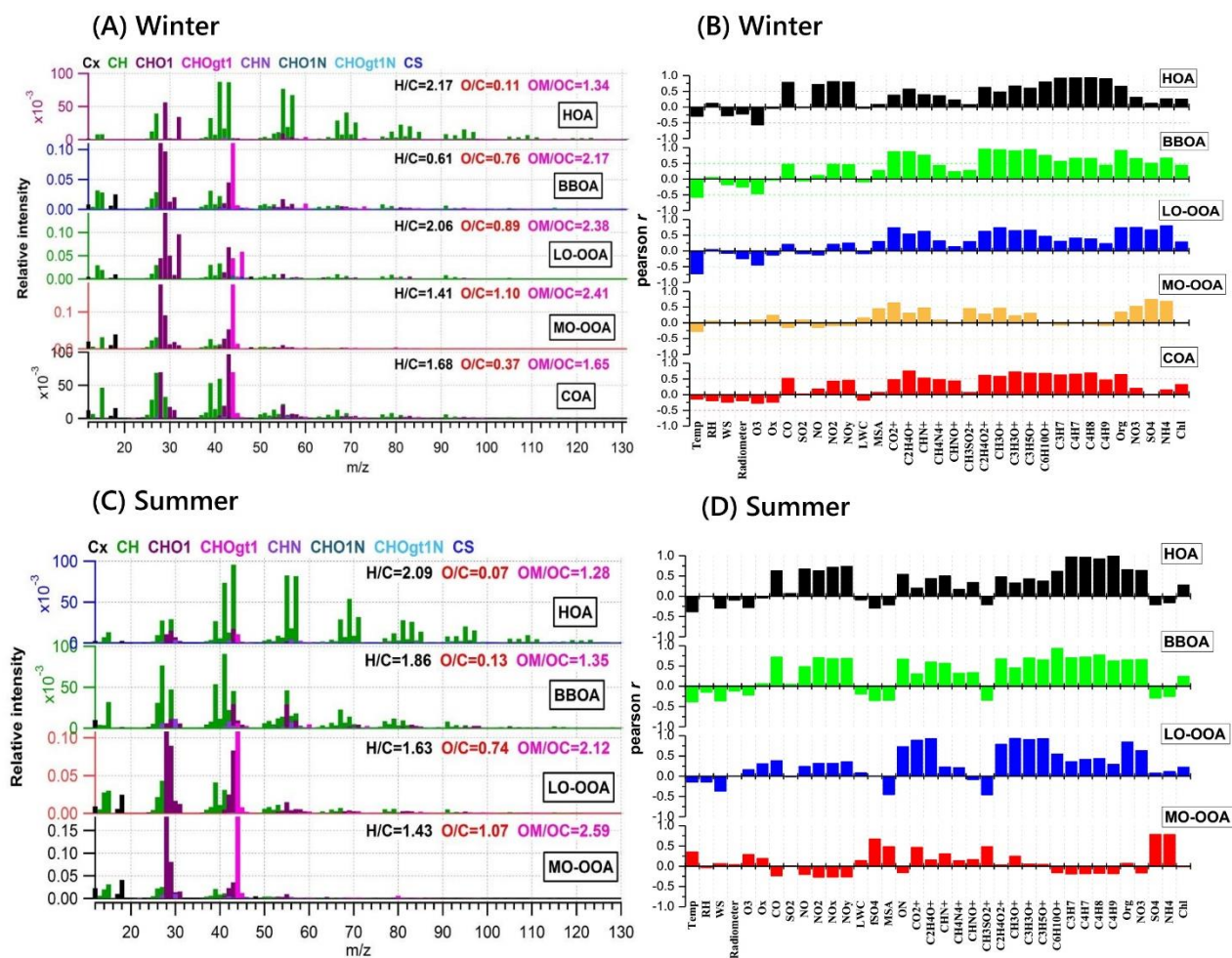


1171

1172

1173 **Figure 5.** Diurnal profiles of the estimated range of nitrate functionality from organic nitrate (A)
 1174 and inorganic nitrate (B) for the winter and summer campaigns. Estimated water associated with
 1175 inorganic and organic aerosol for the winter (C) and summer campaigns (D). Solid lines denote
 1176 the mean value (blue for winter, green for summer), and bars represent the 5/95 percent
 1177 confidence interval in the mean.

1178



1180

1181 **Figure 6.** Mass spectra of PMF-resolved OA factors (A, C) and correlation coefficients between
 1182 OA factors and other variables (tracer ions, trace gas, meteorological parameters, etc.) (B, D) for
 1183 winter and summer campaigns at UHSL.

1184

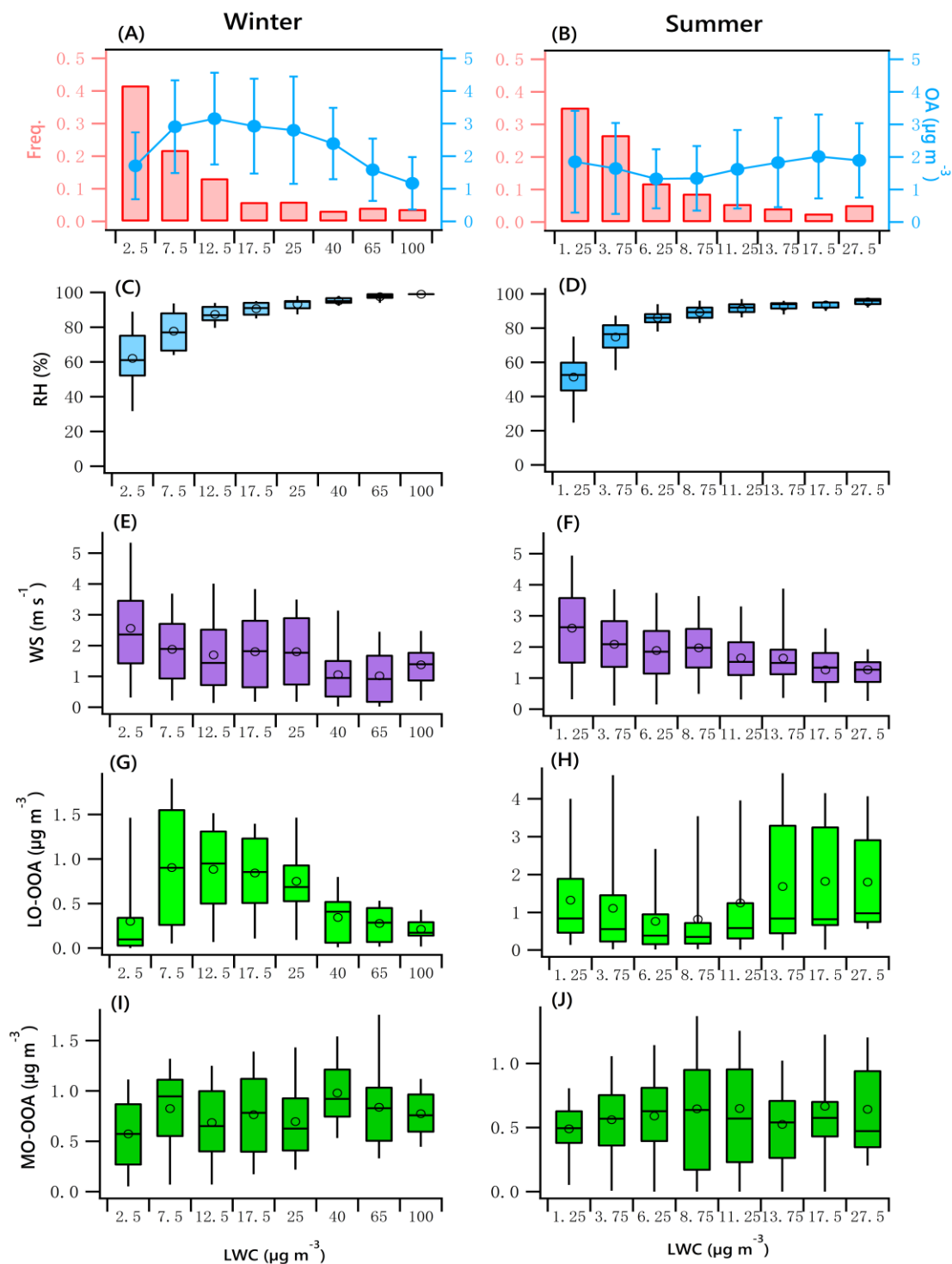


Figure 7. OA mass and frequency histograms of data points in each LWC bin for winter (A) and summer (B). Variations of RH, WS, LO-OOA and MO-OOA mass as a function of LWC in winter (C, E, G, I) and summer (D, F, H, J). The data were binned according to the LWC (with different increment values), and mean (circle), median (horizontal line), 25th and 75th percentiles (lower and upper box), and 5th and 95th percentiles (lower and upper whiskers) are displayed for data in each bin.

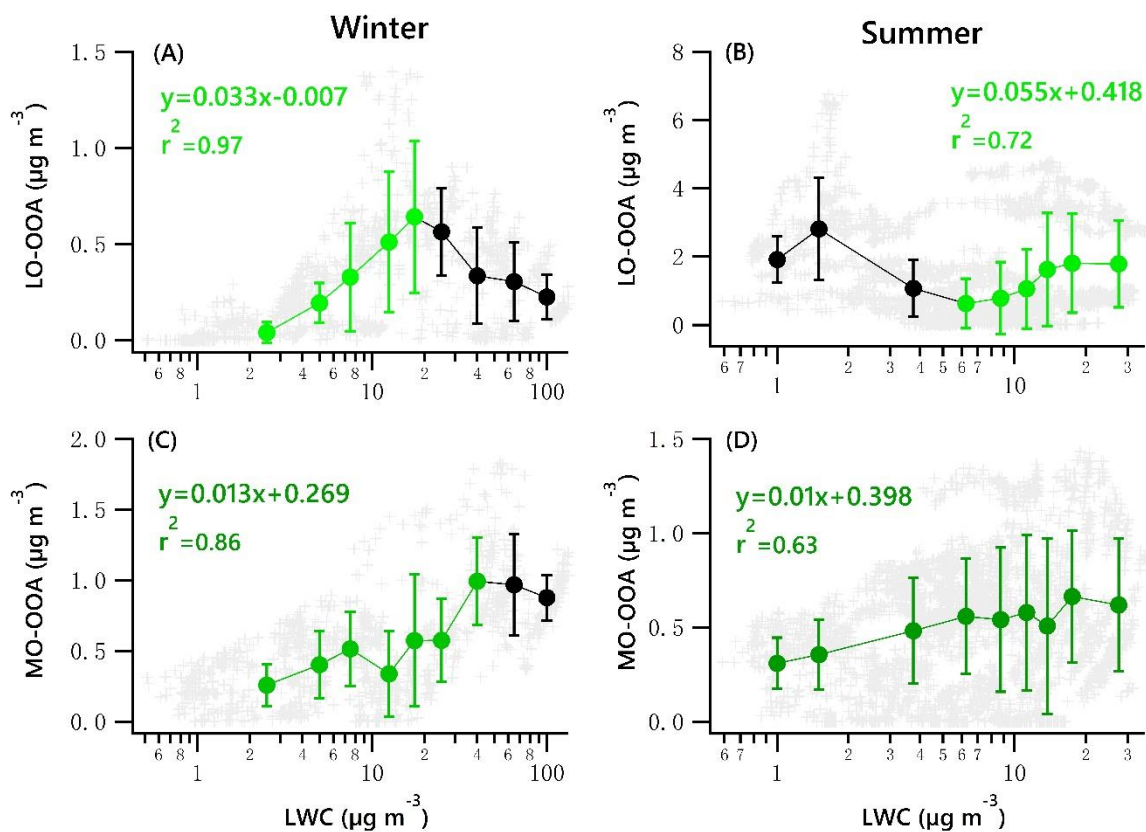


Figure 8. Scatter plots of nighttime OOA vs. LWC for the winter and summer campaign. The linear equations are given for fitting only the green dots. Solid dots denote the average value of data in each bin. Bars indicate standard deviations.

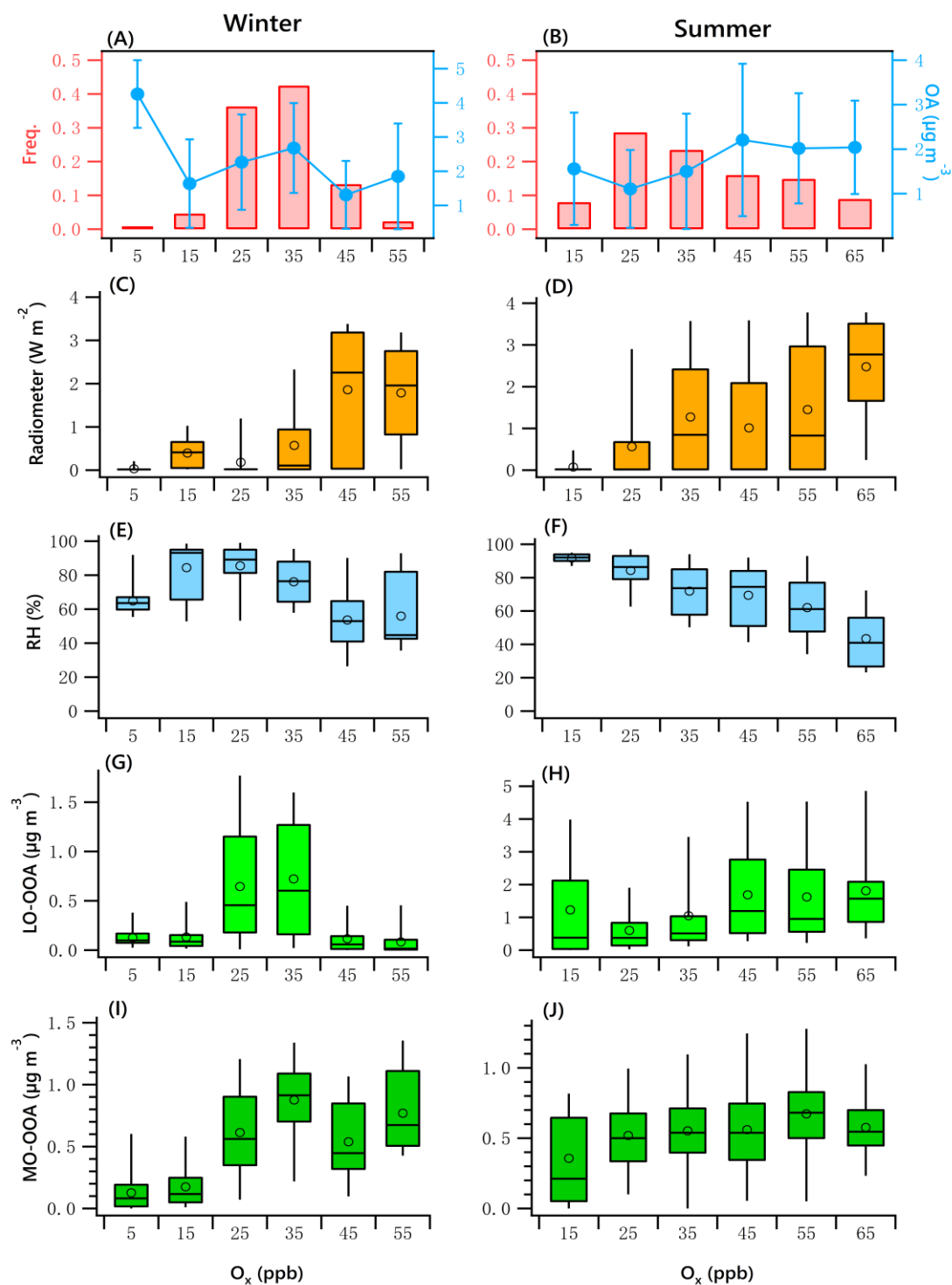


Figure 9. OA mass and frequency histograms of data points in each O_x bin for winter (A) and summer (B). Variations of solar radiation, RH, LO-OOA and MO-OOA mass as a function of LWC in winter (C, E, G, I) and summer (D, F, H, J). The data were binned according to the O_x (10 ppb increment), and mean (circle), median (horizontal line), 25th and 75th percentiles (lower and upper box), and 5th and 95th percentiles (lower and upper whiskers) are displayed for data in each bin.

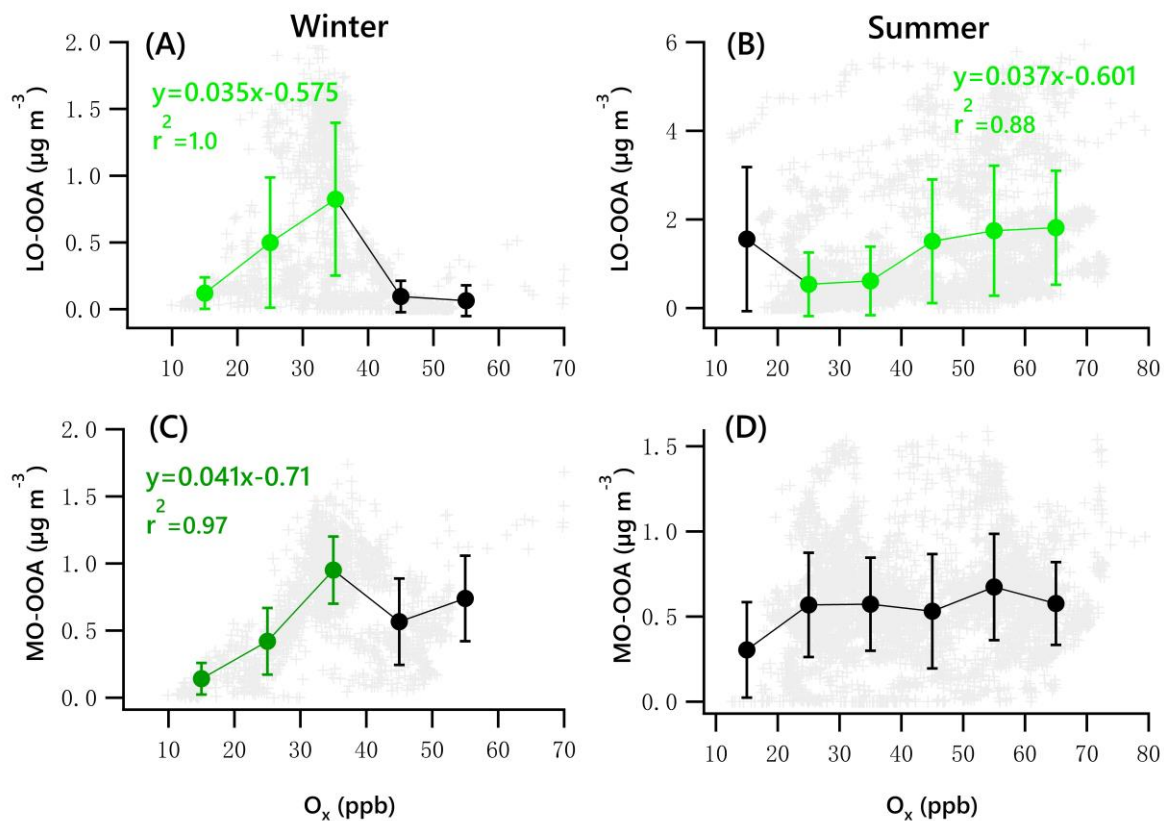


Figure 10. Scatter plots of daytime OOA vs. O_x for the winter and summer campaign. The linear equations are given for fitting the green dots. Bars indicate standard deviations.

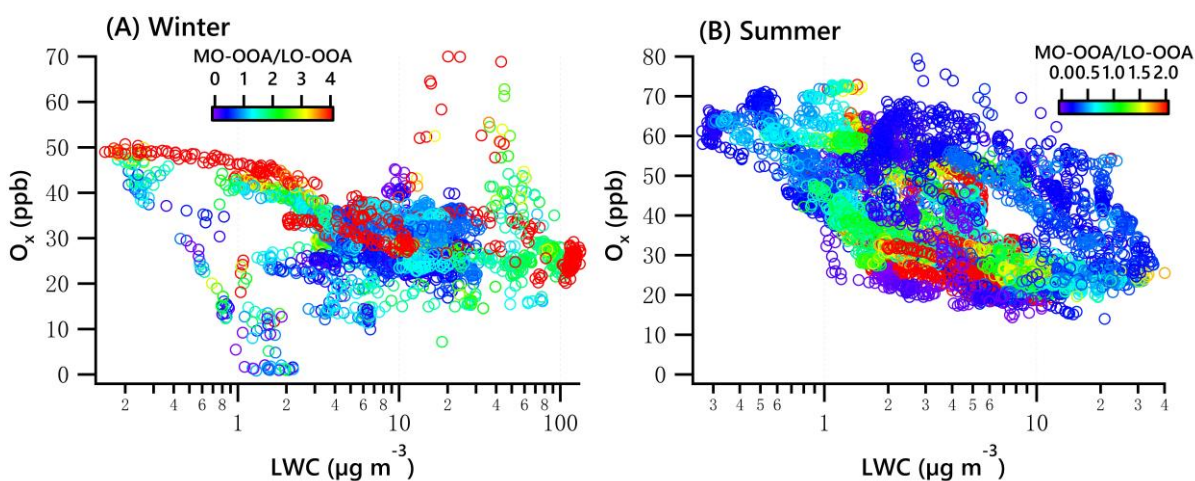


Figure 11. O_x vs LWC dependence of the ratio of MO-OOA/LO-OOA in winter (A) and summer (B).